

# Experimental alluvial fan evolution: Channel dynamics, slope controls, and shoreline growth

Meredith D. Reitz<sup>1</sup> and Douglas J. Jerolmack<sup>2</sup>

Received 31 October 2011; revised 30 March 2012; accepted 2 April 2012; published 16 May 2012.

[1] River deltas and alluvial fans have channelization and deposition dynamics that are not entirely understood, but which dictate the evolution of landscapes of great social, economic, and ecologic value. Our lack of a process-based understanding of fan dynamics hampers our ability to construct accurate prediction and hazard models, leaving these regions vulnerable. Here we describe the growth of a series of experimental alluvial fans composed of a noncohesive grain mixture bimodal in size and density. We impose conditions that simulate a gravel/sand fan prograding into a static basin with constant water and sediment influx, and the resulting fans display realistic channelization and avulsion dynamics. We find that we can describe the dynamics of our fans in terms of a few processes: (1) an avulsion sequence with a timescale dictated by mass conservation between incoming flux and deposit volume; (2) a tendency for flow to reoccupy former channel paths; and (3) bistable slopes corresponding to separate entrainment and deposition conditions for grains. Several important observations related to these processes are: an avulsion timescale that increases with time and decreases with sediment feed rate; fan lobes that grow in a self-similar, quasi-radial pattern; and channel geometry that is adjusted to the threshold entrainment stress. We propose that the formation of well-defined channels in noncohesive fans is a transient phenomenon resulting from incision following avulsion, and can be directly described with dual transport thresholds. We present a fairly complete, process-based description of the mechanics of avulsion and its resulting timescale on our fans. Because the relevant dynamics depend only on threshold transport conditions and conservation of mass, we show how results may be directly applied to field-scale systems.

**Citation:** Reitz, M. D., and D. J. Jerolmack (2012), Experimental alluvial fan evolution: Channel dynamics, slope controls, and shoreline growth, *J. Geophys. Res.*, 117, F02021, doi:10.1029/2011JF002261.

## 1. Introduction and Background

### 1.1. Fans and Deltas

[2] On deltas and alluvial fans, high population densities, broad ecological diversity, and valuable hydrocarbon reservoirs make understanding the underlying deposits and patterns of sedimentation and flooding a matter of public interest [Neill and Deegan, 1986; Syvitski *et al.*, 2005; Reddy *et al.*, 2008]. The ability to forecast fan behavior is especially needed today for predicting the effects of human-induced changes to environmental variables that control fan evolution, such as upstream reduction in sediment supply due to damming, restriction of natural flooding processes by artificial levees, or sea level rise, as these changes may affect the

likelihood of flooding and catastrophic avulsions [Törnqvist, 1994; Syvitski and Saito, 2007; Syvitski *et al.*, 2009]. Deltas forming at the borders between rivers and seas, and alluvial fans between mountains and valleys, are two types of fans. They are distinguished in that due to the nature of their respective sediment sources and boundary conditions, alluvial fans often have steeper slopes and coarser, less cohesive sediment, and deltas have an additional base level dependence on the sea. They are however similar at the broader scale of channelized depositional systems. The process dynamics studied in this paper are common to both systems, but are perhaps more explicitly targeted toward alluvial fans because of the noncohesive sediment, steeper slopes, and lack of a dynamic dependence on sea level.

[3] Experiments and models are useful tools for the study of fan evolution, because in a controlled setting, boundary conditions can be specified and manipulated. Also, because of the decrease in spatial scale from most fans in nature to the laboratory, the temporal scale of their evolution decreases accordingly, and we can observe the establishment and growth of fans in the space of hours or days. Experimental fans have been studied under a variety of boundary conditions, such as tectonic tilting, variable subsidence, and sea level rise [e.g.,

<sup>1</sup>Department of Physics and Astronomy, University of Pennsylvania, Philadelphia, Pennsylvania, USA.

<sup>2</sup>Department of Earth and Environmental Science, University of Pennsylvania, Philadelphia, Pennsylvania, USA.

Corresponding author: M. D. Reitz, Department of Physics and Astronomy, University of Pennsylvania, 209 S. 33rd St., Philadelphia, PA 19104, USA. (mreitz@physics.upenn.edu)

Copyright 2012 by the American Geophysical Union.  
0148-0227/12/2011JF002261

Whipple *et al.*, 1998; Cazanacli *et al.*, 2002; Kim *et al.*, 2006b; Kim and Jerolmack, 2008; Hoyal and Sheets, 2009; Nicholas *et al.*, 2009]. The applicability of the small-scale experimental approach to geomorphic problems has gained acceptance in recent years, as it has been shown that many landscape dynamics do not depend on details of the fluid flow; therefore, the rigorous hydrodynamic similarity that is not generally feasible between experiment and field is less important than a similarity of process [Paola *et al.*, 2009; Malverti *et al.*, 2008; Lajeunesse *et al.*, 2010a]. In this spirit, though our experiments are not meant to reproduce the exact fluid forces in the field, we scale aspects of them in order to study avulsion, the process of large-scale channel jumping, which we will argue is mechanistically similar at the experimental scale.

[4] In this paper, we will detail the evolution of a set of experimental alluvial fans, with a focus on understanding the mechanics of the avulsion process. We will argue that the volume to be filled within an avulsion cycle, which determines the avulsion timescale for a given sediment feed rate, can be described in terms of a separation in slopes, and we will relate this slope separation to a separation in entrainment and distrainment stresses for grains.

## 1.2. Channel Dynamics

[5] *Avulsion.* To first order, fan evolution can be understood in terms of one-dimensional, radially symmetric growth, as the dispersal of incoming sediment on encountering a slope break or after a loss of confinement. Fans can be treated in this broadly averaged spatial manner if they are examined on the order of appropriately broad, geologic timescales [Parker *et al.*, 1998a; Swenson *et al.*, 2000]. The convergence of fan growth toward this radial model at long timescales is accomplished via a rich two-dimensional story of channel formation, migration and abandonment on intermediate timescales [e.g., Hoyal and Sheets, 2009]. This includes the process of avulsion. Because channels are the conduits for water and sediment, sediment deposits more rapidly both within the channel and in the vicinity of the channel than on the surrounding floodplain, and floodplain deposition decreases rapidly with distance from the channel [Pizzuto, 1987; Slingerland and Smith, 2004; Aalto *et al.*, 2008]. This process slowly elevates the channel floor and banks with respect to the floodplain – so-called ‘superelevation’ – until the steeper slope over the floodplain strongly favors the channel’s taking an alternate path [Wells and Dorr, 1987; Smith *et al.*, 1989; Brizga and Finlayson, 1990; Mohrig *et al.*, 2000]. Recent studies of experimental fans show that channels may also avulse with little or no superelevation, due to upstream-migrating waves of aggradation (‘backfilling’) that result from progradation [Hoyal and Sheets, 2009; Reitz *et al.*, 2010]. Regardless of whether superelevation or backfilling is the process driving avulsion, avulsion frequency appears to be related to the time it takes to fill a channel with sediment. For a given channel depth, the avulsion timescale is then expected to scale with the depth divided by the rate of aggradation [Jerolmack and Mohrig, 2007]. Records of periods of increased aggradation rate confirm a positive relationship between avulsion frequency and aggradation rate for both natural [Törnqvist, 1994; Stouthamer and Berendsen, 2001; Jain and Sinha, 2003] and experimental systems [Bryant *et al.*, 1995; Ashworth *et al.*, 2004].

[6] A few experimental studies have focused on the steps of the avulsion process. One set of experiments used a cohesive sediment mixture in an attempt to mimic the effects of fine grains in nature on limiting bank erosion and re-entrainment of deposited grains [Martin *et al.*, 2009; Edmonds *et al.*, 2009; Hoyal and Sheets, 2009]. These studies described an avulsion cycle: Upon avulsing to a new location, a channel is cut into the fan surface, stabilizes, and progrades the shoreline for some time. After a lobe is deposited at the shoreline, deposition within the channel begins at the shore, and a wave of deposition (‘backfilling’) progresses up the fan surface toward the inlet. When the filling channel can no longer contain the flow, water spills over the general surface in a ‘finding phase’. The water selects a new route, into which it then focuses [Schumm *et al.*, 1987; Hoyal and Sheets, 2009; Edmonds *et al.*, 2009]. Clarke *et al.* [2010] built a series of experimental fans from a noncohesive sediment mixture; though the primary mechanism of channel movement was lateral migration, they also observed some avulsions that followed this sequence. Reitz *et al.* [2010] observed the avulsion sequence in fans with noncohesive, bimodal sediment and proposed a mass-conserving relation to predict the avulsion timescale as a function of sediment feed rate and channel geometry.

[7] *Reoccupation.* The tendency of rivers to reoccupy former paths has been observed repeatedly in the field and in stratigraphic records of channel movement [Mohrig *et al.*, 2000; Jain and Sinha, 2003; Aslan *et al.*, 2005]. Aslan *et al.* [2005] proposed that channel reoccupation occurs because previous channels provide ready paths across the floodplain, and because the less cohesive sediments deposited within channels are more easily eroded than the muds and silts of the floodplain. Though these ideas are supported by field observations, they are contrary to original assumptions that previous channels act as topographic repellers because the channel’s elevation above the floodplain would make it more difficult to reoccupy [Leeder, 1978; Allen, 1978]. Channel reoccupation was also observed in a numerical model of fan growth by avulsion, in which avulsion was aggradation-driven and water followed a steepest-descent path [Jerolmack and Paola, 2007]. In a previous paper, we reported various measurements of our experimental fans that indicated channel reoccupation, and presented results of a cellular model that explored channel dynamics in terms of the competition between reoccupation and processes that erase the memory of old channels [Reitz *et al.*, 2010]. We found that reoccupation dynamics were similar to a system in which path selection occurs as a random walk to the shoreline, but channels reoccupy previous paths if they intersect.

[8] Channel reoccupation is a dynamic that has now been observed in the field, in experiments, and in models, but the potential of this knowledge to improve our understanding of bulk fan behavior remains largely untapped.

## 2. Problem Statement and Hypotheses

[9] In this section, we will present background on three motivations for the key hypothesis we will explore in this paper. Our exploration of fan channels indicates that we have stable channels with local geometries out of equilibrium with the incoming sediment flux, which leads us to propose an explanation in terms of a previously described

separation in entrainment and distraintment stresses. The analogue between this separation and the distinction between dynamic and static angles of repose in dry granular systems then leads us to hypothesize that the avulsion sequence on fans is primarily driven by a similar slope fluctuation, resulting from the separation in entrainment and distraintment stresses due to nonuniform transport conditions on fans.

## 2.1. Fan Channels and Thresholds

[10] Because many processes on fans are carried out by channels, understanding channel properties and mechanisms of formation and sediment distribution is an integral part of understanding fan evolution. The transport of grains by water is controlled by stress on the bed, which is partly determined by channel geometry, and transport is in turn responsible for determining the geometry of these channels. Though this interdependence of sediment transport and channelization is complex and not entirely understood, solutions for stable channel depths and widths in equilibrium with incoming sediment and water fluxes have been proposed for various boundary conditions with varying degrees of success [Parker, 1978; Dade and Friend, 1998; Savenije, 2003; Eaton *et al.*, 2004; Diaz *et al.*, 2008]. However, the application of these equilibrium frameworks to systems with heavy spatial and temporal variations in deposition/erosion rates, such as the avulsing channels on fans, may not be justified.

[11] As previously described, for a large part of the avulsion cycle defined in Section 1.2, the upper reach of the channel acts mostly as a sediment bypass system, as deposition begins at the shoreline and the channel slowly backfills; only toward the end of the avulsion cycle does significant deposition occur in the upper reaches and at the apex [Schumm *et al.*, 1987; Hooke and Dorn, 1992; Goedhart and Smith, 1998; Hoyal and Sheets, 2009; Clarke *et al.*, 2010; Reitz *et al.*, 2010]. In order for the geometry of this upper bypass reach to be stable, as it generally is in nature and experiment, the stress on the grains of its bed and banks must be at or below the critical Shields stress for their initiation of motion. The requirement that upper-reach channels must also transport incoming grains of the same type as the grains lining the bed and banks runs up against the ‘canal paradox’. This paradox lies in the apparent inability of a below-threshold channel (as canals are designed) to be able to transport the same type of grains as composes their bed and banks, because this transport would require a stress on the bed in excess of the critical stress for initiation of motion. As a result of this excess, the grains on the bed in the channel center where flow is strongest would be transported; then, grains on the banks would roll down the new gradient to the center. This process would widen the channel unstably [Hirano, 1973; Parker, 1978]. Parker [1978] describes one solution to this paradox, in which a turbulent momentum gradient from the center to the bank of the channel drives a modification of the distribution of stress, which allows banks to be stable (below stress threshold), while the bed is mobile (above threshold). This solution explains well the organization of natural equilibrium gravel bedded streams able to transport grains.

[12] We hypothesize another solution to the paradox, applicable to situations in which channels are not in equilibrium, where there is strong physical justification for separating the behavior of the incoming grain population from that of the embedded grains of the bed and banks.

## 2.2. Separate Entrainment and Distraintment Stresses

[13] Equilibrium channel theory makes an important assumption, which we posit is violated in systems that exhibit strong spatial or temporal variations in deposition, such as channels on fans. The assumption is that grains in motion will immediately distraint (cease moving as bed load and deposit) from the flow upon experiencing a Shields stress that drops below the critical stress for grain entrainment. There is however experimental evidence that grain entrainment and distraintment stresses can be distinct. The separation was reported in the grain-scale studies of saltation presented by Ancey *et al.* [2002], where they write the following description:

[14] “...When a particle was primarily at rest, it could be set in motion by increasing the flow rate beyond a critical value  $q_1$ , but if we then decreased the flow rate, we had to drop it to a value  $q_2 < q_1$  for the motion to cease. The two limits for the threshold of motion reflect a kind of hysteretic behavior of the particle ... This hysteretic behavior is fairly well understood in the context of grain avalanches ... where it has been shown that, for the trapping effect of the roughness to be efficient, the kinetic energy of the particle must be low” [Ancey *et al.*, 2002, p. 6].

[15] In the context of a channel organized to an entrainment threshold, there can be a regime in which the stress on the grains on the bed can have a value lower than the entrainment stress, so that the channels are stable, but higher than the distraintment stress, so that moving particles are transported through. The stress lag is a result of the kinetic energy of the moving grains, and also due to their experiencing a greater drag force and having fewer frictional contacts than static grains in a packed bed. We expect this regime to have non-negligible effects in geomorphic systems with strong spatial or temporal changes in transport conditions. We hypothesize that this applies to alluvial fans because of the strong change in conditions over the fan from the feeder canyon to the valley floor, with a stress lag resulting from the incoming high-momentum grains requiring some time and space to adjust to local transport conditions. At a given local point on the fan, the stress required to entrain a grain from a bed can therefore be distinct (higher) from the stress that will allow the incoming moving grains to be transported through. By invoking separate entrainment and distraintment conditions for grains, we find that there exists a natural solution for stable canal geometries able to transport grains.

## 2.3. Dynamic and Static Angles of Repose

[16] The idea of a separation between grain entrainment and distraintment stresses is strongly preceded by similar dynamics observed in the avalanche hysteresis of dry granular systems, as mentioned in the Ancey *et al.* [2002] quote.

[17] The movement of grains down dry granular piles takes qualitatively different forms depending on the stress at which the pile is agitated. At higher levels of imposed stress, a layer of grains is induced to travel continuously, at a rate that increases as a power law with stress in excess of a critical value, in a manner reminiscent of common bed load formulations [e.g., Bagnold, 1980; Rajchenbach, 1990]. In the lower regime of imposed stress, sediment moves intermittently via recurring avalanches. An avalanche event initiates when the ‘static angle of repose,’ above which grains are able to spontaneously roll, is exceeded; a runaway

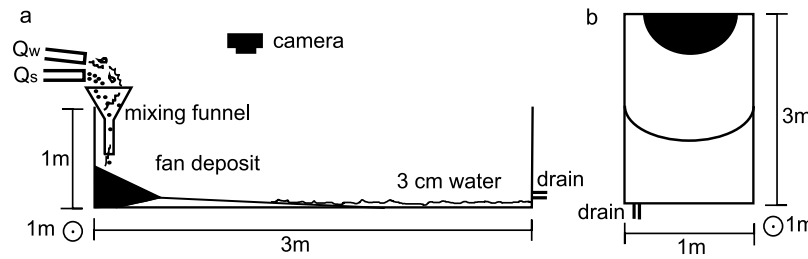


**Figure 1.** (a) Cross-sectional and (b) planview sketches of experimental set-up. A constant bimodal sediment flux ( $Q_s$ ) and water flux ( $Q_w$ ) build a semicircular fan deposit that is bipartite in slope, and progrades into a 3 m length by 1 m width basin of 3 cm standing water. The slope profile is steady in the sense that it maintains an equilibrium slope, but it is continually growing in size throughout the experiment.

mobilization loosens a layer of grains, which fall and settle at a lower, ‘dynamic angle of repose’. Dry granular piles can have aperiodic, power law distributions of avalanche sizes, described by the framework of self-organized criticality [Bak *et al.*, 1987; Tang and Bak, 1988; Grumbacher *et al.*, 1993; Frette *et al.*, 1996]. They can also display periodic avalanche behavior, in which the volume of the loosed granular layer is systematically constrained in some way; the transition between the two avalanche size behaviors has been shown to depend on parameters such as grain sphericity, system size, and characteristics of the base of the pile [Held *et al.*, 1990; Rosendahl *et al.*, 1993; Evesque *et al.*, 1993; Altshuler *et al.*, 2001]. As grains continue to be fed into the system, they fill the volume set by the difference between the static and dynamic angles, gradually backfilling from the bottom of the pile upward, until reaching the static angle and becoming once again susceptible to an avalanche [Jaeger *et al.*, 1989; Rajchenbach, 1990; Buchholtz and Pöschel, 1994; Daerr and Douady, 1999]. This sequence of abrupt avalanching followed by gradual filling results in a series of asymmetric slope fluctuations.

[18] Several of these dynamics of dry granular piles are suggestive of analogies in the systems of deltas and alluvial fans, which are also growing piles of sediment. The water that distributes sediment on fans facilitates its movement by exerting a fluid drag that supplies momentum; the slope expected for a fluid-sheared, channelized pile of sand is therefore much lower than for a dry (or completely submerged) pile. However, they each tend toward predictable and analogous values: the static angle of repose of a dry pile of sand is just below the slope at which grains would roll, and the slopes of natural streams are organized such that grains are close to the critical Shields stress for their initiation of motion [Parker *et al.*, 1998a; Devauchelle *et al.*, 2011]. Typical critical Shields stress values for grains under water are  $\tau_c^* \sim 0.05$  for turbulent flow, or have been reported as high as  $\tau_c^* \sim 0.3$  for laminar flow [Yalin and Karahan, 1979; Buffington and Montgomery, 1997; Lobkovsky *et al.*, 2007].

## 2.4. Hypothesis: Avulsion and a Separation Between Entrainment and Destrainment Slopes

[19] Our key hypothesis is that distinct entrainment and destrainment threshold stresses are expressed on fans in a corresponding slope separation, analogous to the difference between dynamic and static angles of repose in dry systems. We propose that the avulsion sequence of cutting a channel down to entrainment conditions, and filling it by destrainment

of grains from the fan margin backward, corresponds to these two slope conditions. Though slope varies with shear stress but not always in a 1:1 relationship, we cast our arguments in terms of slopes because the slope is the value that in the end most affects the volume being filled within an avulsion cycle. Though the slope associated with distraining grains will likely change as the filling channel forces a wider and shallower flow, the particular slope relevant for setting lobe geometry and formulating the total volume to be filled is the lowest one associated with initial distrainment of grains from the canal-type channel; this is the ‘distrainment slope’ to which we will refer in this paper. Consequences of these distinct thresholds are: (1) bypassed sediment from the upper channel deposits at the fan margin to build lower-slope lobes at the distrainment threshold, and then backfills from the shoreline to the apex, resulting in the documented qualitative avulsion sequence; (2) avulsion timescale is governed by the volume to fill the wedge between critical slopes, and is expected to increase with time and decrease with sediment feed rate; (3) incised channels organize their geometry to that of a stable canal at the entrainment threshold; (4) bulk slope fluctuations will exhibit a pattern similar to that seen for dry granular avalanching; (5) fan slope is insensitive to changes in sediment supply; and (6) the circular distrainment lobes at the shoreline grow in a self-similar manner for reoccupying lobes. In this paper, we quantify and test these predictions using experimental data and simple analytical modeling, and we find strong support for them.

## 3. Methods

### 3.1. Experimental Set-Up

[20] Our experimental fans were built in response to a steady input of  $10^{-6} \text{ m}^3/\text{s}$  sediment and  $5 \cdot 10^{-5} \text{ m}^3/\text{s}$  water. We chose these input values to have a sediment to water ratio safely in the fluvial, rather than debris-flow, regime, and to have the ratio roughly comparable to other experiments [e.g., Sheets *et al.*, 2002; Kim *et al.*, 2006a]; the absolute input values were determined by limitations on our control of water and sediment feed rates. The water and sediment were mixed in a funnel and input as a point source at the center of one end of a 1 m width  $\times$  3 m length  $\times$  1 m depth tank (Figure 1). The height of the fan was not constrained, so that it was free to aggrade with time through the experiment. Because the inertia of incoming grains from canyons onto alluvial fans is a key dynamic factor in nature, we did not attempt to suppress all the inertia of our incoming grains;

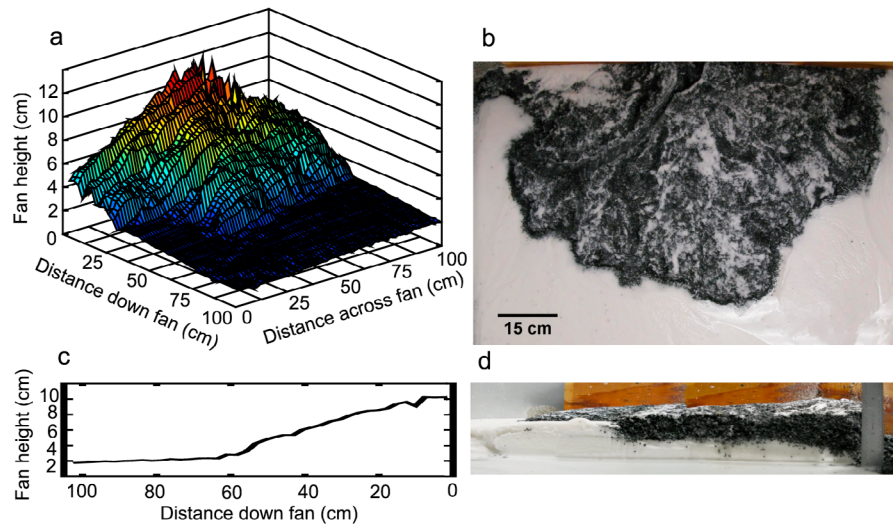


**Figure 2.** (a) Topographic scan and (b) overhead image of the experimental fan of R20 (flow from top to bottom). (c) Fan cross-sectional profile and (d) image (flow in both is from right to left). Coarse black grains deposit first, building a steeper slope, and a sharp coarse-fine slope break, which occurs around 60 cm downstream in this example, progressively progrades over the shallower deposit of fine white grains at an angle of progradation. Fine grains settle out of suspension temporarily on the coarse surface where flow is low, but are only present in final coarse deposit (Figure 2d) in pore spaces between grains.

indeed, we will explicitly address the role played by inertia in our interpretation of the mechanics of avulsion. The method of sediment input did not seem to introduce inertial effects that were excessive to the point of voiding the analogy between the dynamics on our fans and the dynamics on natural fans; we once however tried a different set-up in which sediment was introduced via a ramp, which would have mitigated effects of excessive inertia, but the dynamics and slopes observed were the same as with the funnel method. There was a constant level of 3 cm standing water in the base of the tank, a value resulting from the height of the outlet drain. The boundary of our study area was sufficiently far from the water-sediment interface that the 3 cm value did not impact our analysis. Many alluvial fans in southwest USA exhibit a grain size distribution split between cobbles/gravel, which make up the bed of the steep upper portions of fans, and sand, which deposits on the floodplain, and also on the upper portions of the fan in increasing fractions downfan [Kodoma, 1994; Stock *et al.*, 2008]. We simulated this bimodality using two materials that have approximately the same mobility difference as gravel and sand: black 2 mm granite with a density of  $3.00 \text{ g/cm}^3$ , and white 0.3 mm plastic with a density of  $1.15 \text{ g/cm}^3$ . The aspect of natural bimodality we sought to emulate with this mixture was a separation between populations traveling in suspension and as bed load; we used a Rouse number equivalence, which we discuss in Section 3.2.

[21] Keeping the volumetric water and sediment discharge constant, we varied the relative grain fractions, with values of 5% and 20% granite by volume; we refer to these runs in this paper as R5 and R20, respectively. The strong bimodality of our grain size distribution resulted in strong segregation in their deposition. The coarse grains traveled exclusively as bed load and deposited first to build a steep slope; after an

abrupt transition, the suspended fine plastic grains settled to a shallower slope (Figure 2). The channel dynamics analyzed in this paper took place on the upper, coarse part of the fan. The boundary between these coarse and fine deposit volumes is analogous to the shoreline of a river delta, or the gravel-sand transition seen in natural rivers [e.g., Sambrook Smith and Ferguson, 1995] and, we argue, on many natural fans. The presence of fine grains in the coarse deposit served the purpose of filling pore spaces, so that water flowed overland, rather than through the deposit; we found that volumetric fine fractions of less than 80% resulted in non-negligible water infiltration. Fine grains also deposited as an inert dusting on the coarse surface where flow over an area was slow and shallow. The surface fraction of fine grains increased downfan in a manner similar to sand on natural fans [Stock *et al.*, 2008].

[22] The coarse fans built until they reached the width of the tank, so the final deposits had a diameter of about 1 m. Because sea level was constant and sediment was being constantly introduced, the fans were growing in size throughout the experiments. After an initial spin-up time, the fans settled into a ‘dynamic equilibrium’, in which the studied avulsion processes were regular; all of our quantitative measurements, except for our continuous shoreline mapping, were taken within this regime. R5 lasted  $\sim 25$  h and R20 lasted  $\sim 15$  h. Because the two fans behaved similarly, we focused on the dynamics within one run, R20, for much of our analysis. R5 was also analyzed to test the dependence of observed dynamics on sediment feed rate.

[23] Our primary form of data collection was aerial images taken every 2 min. We also used an Acuity AccuRange AR700 laser with a vertical resolution of  $\pm 1$  mm to take full topographic scans 2–3 times per run. These scans were taken when the water was turned off, with a downstream

**Table 1.** Summary of Parameters and Measured Quantities of Experiments<sup>a</sup>

	$Q_w$ (cm <sup>3</sup> /s)	$Q_s$ (cm <sup>3</sup> /s)	$Q_{s, \text{fine}}$ (cm <sup>3</sup> /s)	$h$ (cm)	$B$ (cm)	$S$	$u$ (cm/s)	$Fr$	$Re$	$\tau^*$
R5	50.47	0.05	0.95	0.93	5.63	0.19	9.64	0.32	896	0.43
R20	50.47	0.2	0.8	0.52	6.32	0.17	15.4	0.64	799	0.22

<sup>a</sup>Water flux  $Q_w$ , coarse sediment flux  $Q_s$ , average measured channel depth  $h$ , average measured channel width  $B$ , bulk measured slope  $S$ , estimate of water velocity  $u$  from continuity equation, calculated Froude number  $Fr$ , calculated Reynolds number  $Re$ , and calculated dimensionless stress on bed  $\tau^*$ . All measurements of these quantities (and of quantities in other tables) were taken after the equilibrium slope had been established and the avulsion dynamics had become regular.

resolution of 2.5 cm per point and a transverse resolution of  $\sim 0.4$  cm per point. In one run we repeated the topographic scan of a single cross-section every 5 min.

### 3.2. Experimental Scaling

[24] Researchers often try to match either the Reynolds or the Froude number between systems, in the attempt to create similar transport conditions between experimental and natural scales. Our experimental channels have subcritical Froude numbers (Table 1) that are reasonable for alluvial rivers and delta channels, but conflict with some alluvial fan studies that observed supercritical flow, so that in this aspect, our experiments may not be directly scalable to natural fans [Rahn, 1967; Beaumont and Oberlander, 1971]. However, because our process arguments are focused on bulk grain mechanics that are not likely to depend strongly on Froude-related hydrodynamics, a conflict in Froude scaling would be acceptable for the purposes of our study. Our Reynolds numbers are around 800 (Table 1), so our channels are likely in a transitional regime between laminar and turbulent flow [Peakall et al., 1996; Lajeunesse et al., 2010a]. Either turbulent or laminar flow is acceptable for the study of our chosen problem. If flow is turbulent, then ‘Reynolds-number independence’ allows for the comparison between our channels and natural channels, which are also turbulent, but at much higher Reynolds numbers [Paola et al., 2009]. It is also acceptable if flow is laminar, because it has been demonstrated that the fundamental processes of bed load transport are similar between laminar and turbulent flows [Malverti et al., 2008; Lajeunesse et al., 2010b].

[25] For the scaling of our experiments, we focus more on certain aspects relevant for transport and pattern formation: the separation between coarse populations traveling as bed load and fine populations in suspension, the organization of slope to an equilibrium value, and the separation of scales that allows studies of avulsion to overlook smaller-scale processes that are more sensitive to scaling issues. An appropriate scale parameter for grain mobility is the Rouse number; we find

Rouse similarity (Table 2) between channelized flows in our experiments and on the natural alluvial fans reported by Stock et al. [2008]. The fine grain populations of plastic in our experimental fans and sand on natural fans are in the fully suspended regime in each system, while coarse populations are in the pure-bed load transport regime; we observe this separation during the experiments. Another scale-independent similarity that we propose between channels on our experimental fans and channels in nature is an adjustment to a near-threshold state in terms of slope and channel geometry in order to pass the imposed coarse-grain load. Though there is evidence of such organization for natural inland bed load channels, which prompts the use of this assumption in alluvial fan modeling scenarios [Parker et al., 1998a], testing of this assumption for the case of channels on fans has shown mixed support [Jerolmack and Mohrig, 2007; Stock et al., 2008]. We will however use this assumption in our analysis, and interpret that a correspondence in threshold organization between our fans and natural fans results from the mechanics of similarly driven avulsion sequences. Finally, we argue that because the dynamics of avulsion act across broad time and space scales and are driven by mass conservation, they will not depend strongly on details of within-channel transport. Because of this separation of scales, avulsion mechanics can be studied somewhat independently of potentially unscalable processes that influence smaller time and space scales [Paola et al., 2009; Reitz et al., 2010].

### 3.3. Methods of Analysis

[26] *Image processing.* Most of our analysis was done via image processing, using the NIH-developed software ImageJ. By taking the difference between successive images, we could isolate the areas of change on the fan, which corresponded to water locations because of moving water, grains, and bubbles (Figure 3b). Then, by thresholding and blurring these differenced images, we converted these images to binary maps of water location (Figure 3c). The black and white colors of our grains also let us easily discern grain sorting patterns

**Table 2.** Comparison of Rouse Numbers of Grain Size Populations Between Natural Alluvial Fans and Our Experimental Fans<sup>a</sup>

	$h$ (cm)	$S$	$Ro, \text{ sand } \approx 0.03$ (cm)	$Ro, d_{50} = 2.07$ (cm)	$Ro, d_{84} = 5.51$ (cm)	$Ro, \text{ plastic } = 0.03$ (cm)	$Ro, \text{ granite } = 0.24$ (cm)
Natural fans	60	0.049	0.193	3.08	5.08		
R5	0.93	0.19				0.106	4.07
R20	0.52	0.17				0.148	5.70

<sup>a</sup>Here  $Ro = w_s/(\kappa u^*)$  (dimensionless). The grain settling velocity  $w_s$  is calculated with the Ferguson and Church [2004] formulation,  $w_s = \frac{Rgd^2}{C_1 v + (0.75 C_2 Rgd^3)^{0.3}}$ , where  $C_1 = 18$  and  $C_2 = 1$  for natural grains,  $R$  is the relative submerged density of the grains,  $d$  is the grain diameter, and  $v$  is the kinematic viscosity of water. The shear velocity  $u^*$  is estimated from the depth-slope product,  $u^* \approx \sqrt{ghS}$ , where we use  $h$  measured within the channels and  $S$  the average measured coarse fan slope, and  $\kappa$  is von Kármán’s constant, 0.41. The data for natural fans is averaged over the four alluvial fans described in Stock et al. [2008]. Because the Stock et al. [2008] data set does not include measurements of sand grain size, the estimate of 0.03 cm diameter is used. The fine populations have Rouse numbers in the suspended regime, while the coarse populations are transported as bed load, consistent with our observations during the experiment.



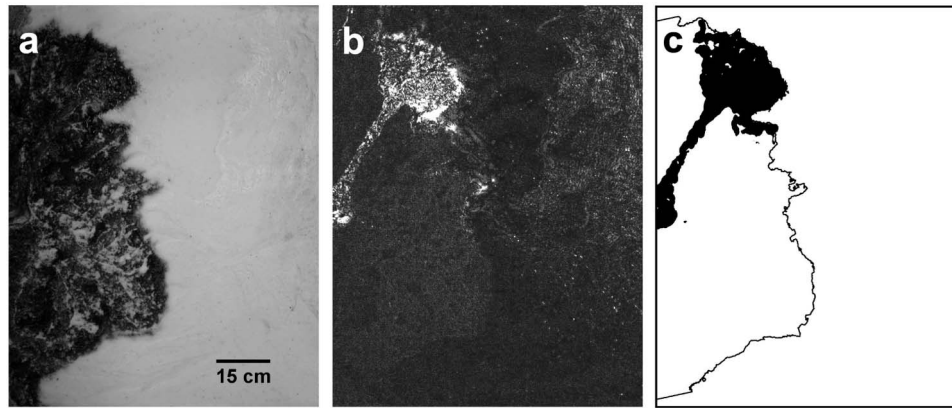


**Figure 3.** Sequence of image processing steps, with images from R20. (a) Image of fan deposit, where coarse grains are black and fine grains are white. (b) Difference between Figure 3a and the image of the fan taken two minutes earlier. Because of moving water and bubbles, the location of the channel shows up as white against the dark gray background. (c) Thresholding and blurring the differenced image of Figure 3b, we create a binary image of channelized area. Also shown in this frame is the fan margin extracted from the clear coarse-fine boundary in Figure 3a.

from aerial images, and we used the contrast between these colors to trace the coarse fan margin (Figure 3c). We verified these methods visually, through comparison to raw images and direct observation. Because the processing involves thresholding and blurring, the determination of flow boundaries was not absolute, but for the pattern description purposes of our paper, it was sufficient.

[27] *Slope measurements.* We employed both direct and indirect measures to quantify the slopes of our alluvial fans. Directly, we quantified the slope 3–5 times for each experiment by using our full topographic scans. These were profiles averaged down the central 10 cm of the final fan deposit. The reason for not using the entire radial average was that the sinuosity of the lobes at the shoreline resulted in the slope break between the coarse and fine grain deposits being unrealistically smoothed out in the radial average. A robust result is that fan profiles are linear, i.e., they exhibit very little curvature.

[28] Because the temporal resolution of our aerial image data set was much higher than our topographic data set, and we wanted to quantify slope fluctuations through time, we also employed the indirect measure of estimating the overall slope from the mean radius location obtained from the aerial photos. We combined this mean radial growth with the sediment influx and the approximation of a conical fan volume. This method then allowed us to generate a time series of estimated fan slopes throughout a run. The average growth relation for the radius of a half-cone is:

$$r(t) = \left( \frac{6Q_s}{\pi S} \right)^{1/3} t^{1/3} \quad (1)$$

where  $r$  is fan radius growing with time  $t$ ,  $S$  is fan slope, and  $Q_s$  is sediment supply. For our fans, we also needed the angle of progradation of the coarse-grained fan over the deposit of fine grains (marked as  $\alpha$  in Figure 2), and an estimate of coarse sediment porosity. To estimate our coarse grain porosity, we compared the directly measured slope value with slopes estimated using (1) and the measured angle of

progradation ( $\sim 4^\circ$ ). This  $t^{1/3}$  scaling is appropriate here because of the non-negligible slope of our fans, while studies of natural deltas with very low gradient topsets scale more closely to  $t^{1/2}$  [Wolinsky *et al.*, 2010].

[29] *Avulsion timescale metrics.* We used four metrics to estimate the avulsion timescale. Two were direct measurements which we relate to steps in the observed qualitative pattern of avulsion: the frequency of pulses in the average fan margin position, where a pulse corresponds to the lobe-building phase, and the frequency of the fluctuations in the fraction of the fan surface covered by water, where a high fraction corresponds to the flooding phase. The other two were statistical measures of the movement of water, which give avulsion timescales because avulsion has a systematic influence on flow behavior: the measures of the channel decorrelation time and the rate of decay of the dry fraction. The distribution of channel decorrelation times gives the distribution of times it takes for currently wetted pixels to go dry, and is a bulk measure of channel mobility. The rate of decay of the cumulated dry fraction of the fan is a measure of the time it takes for channels to fill space over the fan. We compared all four measurements of the avulsion timescale for R20, to demonstrate consistency among the methods. We then selected one method to compare between runs and to look in greater detail at the magnitude of change in the avulsion timescale through time.

## 4. Results

### 4.1. Observed Fan Behavior

[30] In response to steady water and sediment influx, our fans exhibited a rich set of autogenic processes. Selective deposition resulted in strong grain size sorting and an abrupt coarse-fine transition, and the coarse fan steadily prograded over the fines (Figure 2). Since we propose that this transition is analogous to a transition from gravel to sand on natural rivers, the shoreline of a river delta, or the outer margin of alluvial fans, we refer to the coarse-fine boundary in our experimental fans as the ‘fan margin’.

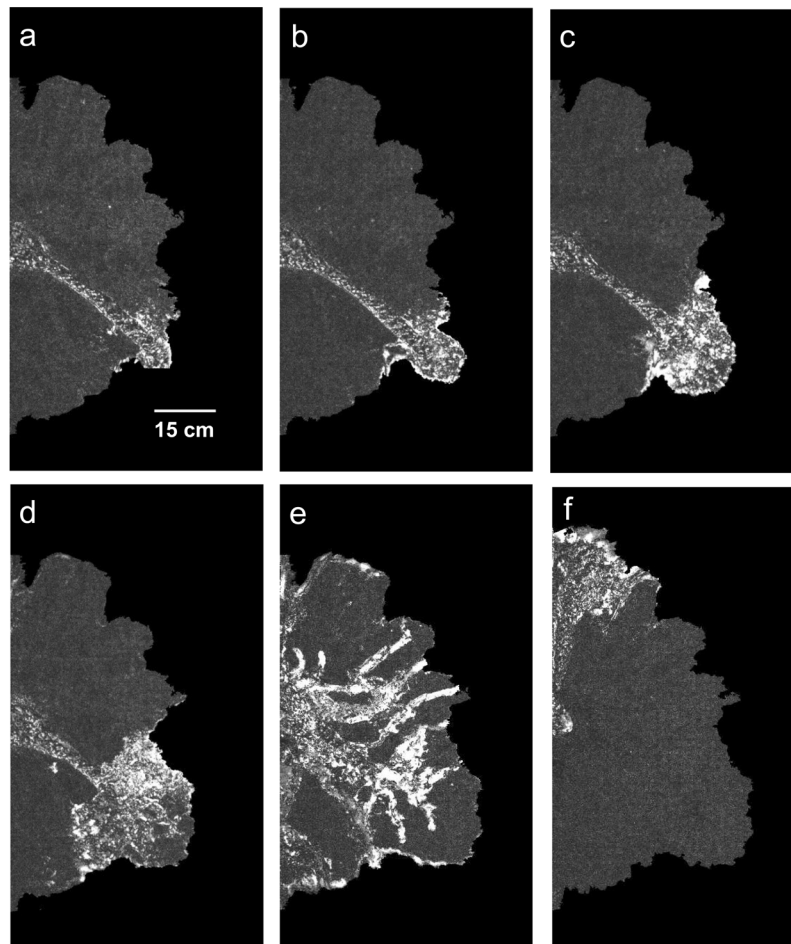


**Figure 4.** Avulsion sequence observed in our experiments. Images shown here are differences between successive frames in R20 (time interval is 2 min); the dark gray area is the coarse fan, while the locations of water are white due to the movement of bubbles, water and grains between frames. The system recursively (a) strongly channelizes, (b) pushes out the shoreline, (c) flares out locally to establish a semi-circular lobe, (d) backfills, (e) floods, and (f) channelizes.

[31] During the initial stage of an experimental run, the coarse fan deposit was a steep pile built by unconfined flow that covered a large fraction of the surface, while the fine grains settled to begin to establish a submerged downstream blanket of sediment. The fan continued to build, with the coarse fan deposit prograding over the deposit of fine grains and the fine grains eventually building up to breach the surface of the 3 cm of standing water in the basin. We refer to the initial stage before the onset of regular channelization as the ‘spin-up time’; for R20 for example, this stage lasted for the first 200 min of the experiment. Thereafter, the channelization process observed on our fans was one of successive avulsions, which followed a well-defined pattern.

[32] The initial phase in the avulsion sequence was a quick focusing of flow from a flood into a narrow channel (Figure 4a). The measured fraction of the fan covered by water (‘wet fraction’) abruptly dropped in this phase, and the fan margin pushed out as the channel built a lobe, resulting in a pulse on the growth of the mean fan margin. We observed in our experiments that lobe establishment took place in regions newly channelized by avulsions; to watch the progression of shoreline contours through time as the

building lobes relocate in connection with avulsing channels, see Animation 1, or for a video of image differences that allows visual comparison between avulsion and lobe building see Reitz *et al.* [2010, Animation S1].<sup>1</sup> The establishment of lobe geometry happened relatively quickly (Figures 4b and 4c). Following lobe establishment, the focus of deposition was seen to slowly progress back from the fan margin toward the apex, as the channel filled in available space between the lobe margin and the apex, including the space within the channel itself (Figure 4d). When the channel was filled with sediment, the unconfined flow broke into a flood over the fan (Figure 4e). A new route was selected, and the sequence repeated (Figure 4f).

#### 4.2. Reoccupation and Fan Margin Growth

[33] The channels we observed radiated from the apex, with each lobe subtending an angle of approximately  $36^\circ$ , or  $\pi/5$  radians, establishing a network of 4–5 channel paths. As reported in our previous paper, we observed the maintenance of this channel network as avulsing channels showed

<sup>1</sup>Animation is available in the HTML.



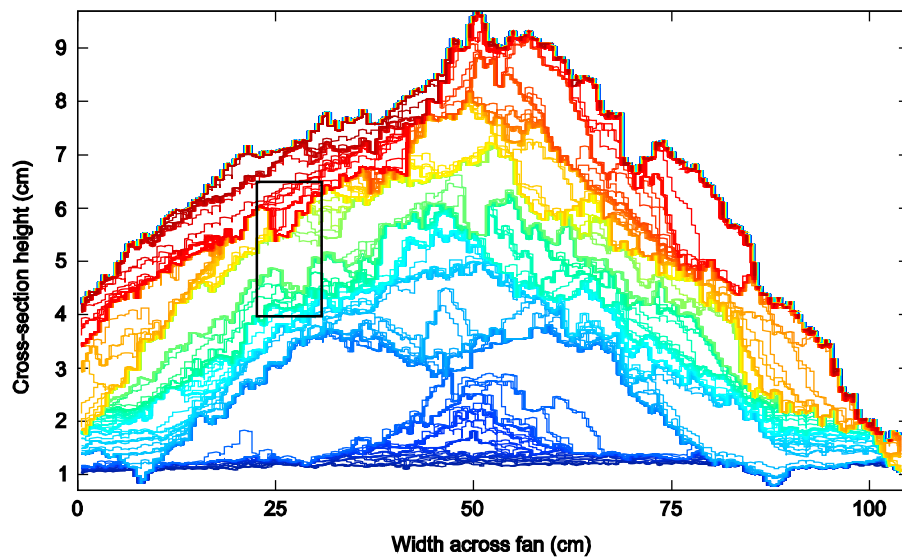


**Figure 5.** The cumulated stratigraphy of one cross-section through time, plotting contours of deposited sediment that was not subsequently eroded, at a location approximately 20 cm downstream of the fan inlet. Scans (contours) were repeated every five minutes. The gap near 2 cm height is due to missing data. The colors from blue to red represent the progression through  $\sim 15$  h of R20. This cumulated stratigraphy map contains information about channel dynamics, including channelization, channel filling, and channel reoccupation (boxed example).

a marked tendency to reactivate former flow paths [Reitz *et al.*, 2010]. As an example illustration of this effect, we plot the cumulated stratigraphy of one cross-section from a series of 5-min interval repeat topographic scans in one place, which plots contours of sediment deposited at a given time that was not subsequently re-eroded, analogous to a map of a stratigraphic cross-section. In this map, we can see examples of the reoccupation of channels that had previously been filled (Figure 5).

[34] One pattern dictated by channel path selection behavior is the manner of fan margin growth (Animation 1). In composite images of the fan margin contours throughout an experiment, channel locations are visible as lobe growth locations. Fan margin growth primarily occurred via the

revisiting and enlargement of existing lobes (Figure 6a). (Though the number of lobes stayed roughly constant through our experiment, this number would likely start to increase with radius at some scale, at least when lobe size begins to approach the size of our fans.) For the purpose of examining these maps, a reoccupation event was defined visually as a lobe that subtended the same angle as the previous occupation in the region. We observed reoccupation to be a tendency, not a deterministic behavior, so that not all lobes visible in Figure 6a are reoccupying former paths, but there are several clear examples where they do.

[35] Since we observed that lobe geometry tended to be circular with respect to a local radius of curvature much smaller than the fan radius, we can use this local circularity as

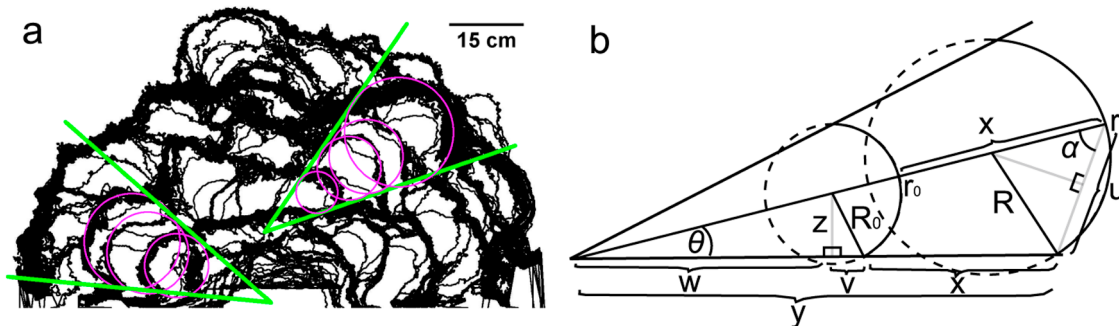


**Figure 6.** (a) Two-minute contours of the growth through time of the fan margin of R20 show that existing channel lobes get revisited and enlarged, as in the two indicated examples of reoccupied lobes. Thick black lines mark locations where the shoreline persisted in one place for an extended period of time, while thin lines represent single contours and show the rapid progradation that occurs during lobe formation. (b) A map view sketch of the relevant variables of (2), including the fan radius  $r$ , lobe radius of curvature  $R$ , opening angle  $\theta$ , and initial fan radius  $r_0$  and lobe radius of curvature  $R_0$ .

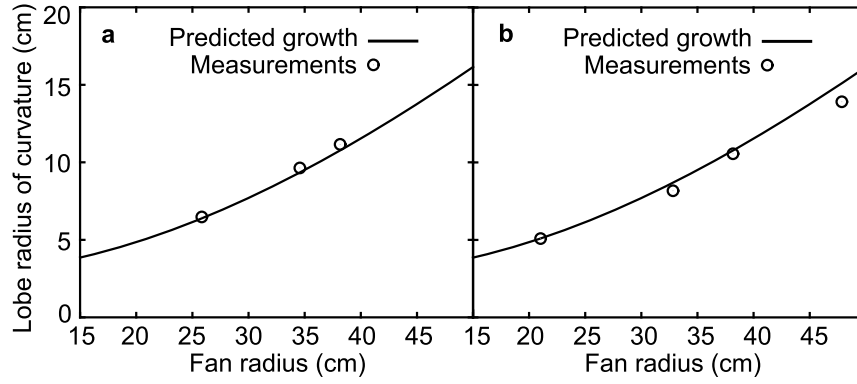


**Figure 7.** Comparison of predicted evolution of lobe radius of curvature with measured values, for the (a) left and (b) right highlighted lobes of Figure 6a. The first point on each plot is used to calibrate the curve, but subsequent lobe evolution is well predicted by (2).

a constraint to allow us to make geometric predictions about the manner of lobe growth for the case of reoccupying channels. Fan margin growth is then subject to the conditions that: (1) channels reoccupy former paths; (2) average growth must be radial with respect to the fan apex; and (3) lobe geometry is locally semicircular. These conditions are sufficient to describe the growth of lobe radius of curvature with fan radius.

[36] We solve for the evolution of lobe radius of curvature  $R$  with fan radius  $r$ , given initial  $R_0$  and  $r_0$  and the opening angle  $\theta$  (Figure 6b; see Appendix for intermediate steps). The final result is a simple though awkward equation for  $R(r, r_0, R_0, \theta)$ :

$$R = \frac{1}{2} \left\{ 1 - \frac{\sin^2 \theta \left( r + r_0 \cos \theta - R_0 - r_0 + \sqrt{R_0^2 - r_0^2 \sin^2 \theta} \right)^2}{\left( r + r_0 \cos \theta - R_0 - r_0 + \sqrt{R_0^2 - r_0^2 \sin^2 \theta} \right)^2 + r^2 - 2r \left( r + r_0 \cos \theta - R_0 - r_0 + \sqrt{R_0^2 - r_0^2 \sin^2 \theta} \right) \cos \theta} \right\}^{-\frac{1}{2}} \cdot \left[ \left( r + r_0 \cos \theta - R_0 - r_0 + \sqrt{R_0^2 - r_0^2 \sin^2 \theta} \right)^2 + r^2 - 2r \left( r + r_0 \cos \theta - R_0 - r_0 + \sqrt{R_0^2 - r_0^2 \sin^2 \theta} \right) \cos \theta \right]^{\frac{1}{2}}. \quad (2)$$

We test this predicted evolution using measurements of two reoccupied lobes on our experimental fan (Figure 7). We find agreement with the predicted evolution. The confirmation of this geometric growth supports our assumptions, indicating that (1) reoccupation can be used as a condition for projecting shoreline growth patterns, and (2) while overall growth is radial with respect to the apex, lobe growth is also fundamentally constrained by the circular filling of space.

#### 4.3. Self-Organization of Channels and Fan Slope

[37] *Threshold channel geometry.* Our fans exhibited strong channelization, with self-formed banks incised into the fan topography, and no detected levees. Measured channel depths  $h$  and widths  $B$  are reported in columns (c)–(d) of Table 1. Each reported value is an average of the measurements of at least five different channels, taken in the upper ‘bypass’ reaches. We did not see a trend of changing channel geometry with time. Our topographic resolution was not high

enough to determine channel cross-sectional shape, so we have presented single numbers as representative channel depths and widths. We found that measured channel geometries did not vary much between R5 and R20, though coarse sediment supply was varied by a factor of four. This finding contrasts with equilibrium channel theory, which predicts an interdependence between channel geometry and sediment supply [e.g., Parker, 1978], but is consistent with a canal geometry control.

[38] We compute the expected equilibrium canal geometry for our channels using the Savenije [2003] theoretical rederivation of the empirical Lacey canal formulae, which seems to be generally applicable to straight reaches of stable

threshold channels. The derivation uses the sinusoidal shape of a stable threshold channel, for which gravity and fluid drag are in balance, to solve for the relation between mean channel depth ( $h$ ) and width ( $B$ ):

$$h = \frac{2 \tan \varphi}{\pi^2} B, \quad (3a)$$

where  $\varphi$  is the angle of repose of the bed material. This equation can be combined with the water continuity equation  $Q_w = uhB$ , to give:

$$B = \sqrt{\frac{\pi^2 Q_w}{2u \tan \varphi}}, \quad (3b)$$

where  $u$  is the average bankfull within-channel velocity and  $Q_w$  is water flux. Since we did not directly measure flow velocity, but estimated it with the continuity equation,

**Table 3.** Channel Geometries of Our Experimental Fans, Compared With Predictions of the *Savenije* [2003] Threshold-Channel Framework<sup>a</sup>

	$h$ (cm)	$B$ (cm)	Savenije $h$ (cm)	Savenije $B$ (cm)
R5	0.93	5.63	0.91	5.74
R20	0.52	6.32	0.72	4.55

<sup>a</sup>Where  $h$  is channel depth,  $B$  is channel width, R5 is the run with 5% coarse material, and R20 is the run with 20% coarse material.

(3b) for us is more a consequence of (3a) than an independent measurement. We measured the angle of repose of our grains to be  $38^\circ$ .

[39] In our experiments, measured channel geometries corresponded closely to these canal formula predictions (Table 3). In contrast, using the *Parker* [1978] equilibrium gravel bedded stream equations with our critical Shields stress of 0.3 predicted an unrealistic slope of 2.24 for our measured channel depth, or unphysical (negative or imaginary) channel depths for our measured slopes. These calculations support our hypothesis that these out-of-equilibrium channels organize to the entrainment threshold.

[40] *Fan slope dynamics.* From our topographic scans, we measured the fan slope 3–5 times for each experiment. We found that while there was some variation, these slope measurements were generally consistent, and did not show a trend of change through time or with gravel fraction. The average slope for R5 was 0.19 (range 0.16–0.23), and the average slope for R20 was 0.17 (range 0.16–0.20).

[41] For an estimate of the porosity of our coarse-grain deposits, here we compare the measured slope value with slopes estimated using (1), and the angle of progradation ( $\sim 4^\circ$ ). We observed in R20 (Figure 8) that the slope estimated in this way decreased over the spin-up timescale of  $\sim 200$  min to reach an equilibrium value, around which it

fluctuated for the rest of the experiment. Since the equilibrium slope values between the two runs were similar, we used a representative value of 0.2 for our calculations. This value produces an estimated porosity of 0.5 for run R20; we apply this value for R5 as well, where experimental challenges made the shoreline position difficult to resolve. The deposit cross-sections between the two runs did not show a noticeable porosity difference.

[42] The magnitude of total slope fluctuations within one run was  $\sim 10\%$  of the slope value (Figure 8 inset). The magnitude of these fluctuations was slightly less than the magnitude of variation in our direct slope measurements; this is likely because the direct measurements were over a subsection of the fan, whereas the conical slope estimates use the average radius of the entire fan, and slope variation can be larger on a local scale. The fluctuations of Figure 8 are reminiscent of those seen in other noncohesive fan experiments [Kim *et al.*, 2006a; Kim and Jerolmack, 2008], although fluctuations there were of a smaller magnitude (1–4%). In R5, the trend showed a longer timescale to equilibrium, of approximately 400 min. The equilibrium slopes were reached approximately 25–30% of the way through the runs, which were stopped when the coarse fan neared the width of the tank. The steady slope value was therefore not a result of a boundary condition where the edge of the tank removed incoming sediment, but resulted rather from internal fan dynamics. We also observed that the equilibrium time of  $\sim 200$  min in R20 was the time at which the avulsion cycle became regular in the sense of following the sequence steps described in the introduction. This covariance is consistent with the idea that the avulsion cycle itself could be responsible for the slope self-regulation, which would fit with our interpretation.

[43] We can now calculate the theoretical growth relation (1). Using our measured slope value, and adjusting

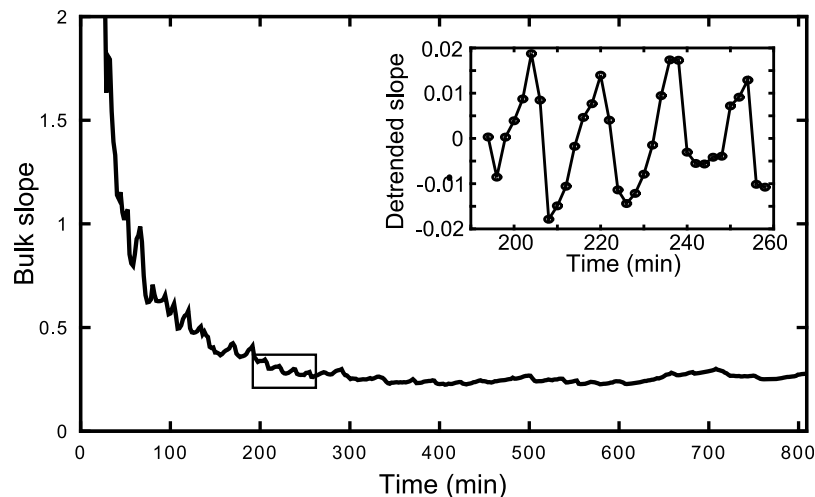


**Figure 8.** Bulk slope of R20 fan (unitless ratio), calculated with the average fan margin position and the volume influx of sediment, assuming a conical shape (1). After a time of  $\sim 200$  min, the slope reaches the equilibrium value of  $\sim 0.2$ , the same value obtained by topographic scans (Table 1). The (inset) sawtooth shape of detrended slope fluctuations are reminiscent of the fluctuations of the avalanching slopes of dry granular piles (e.g., sawtooth sandpile mass fluctuations of *Held et al.* [1990, Figure 2d]), in that the slope slowly increases before reaching a threshold value, and abruptly decreases as stored sediment is released and the mean fan margin extends.

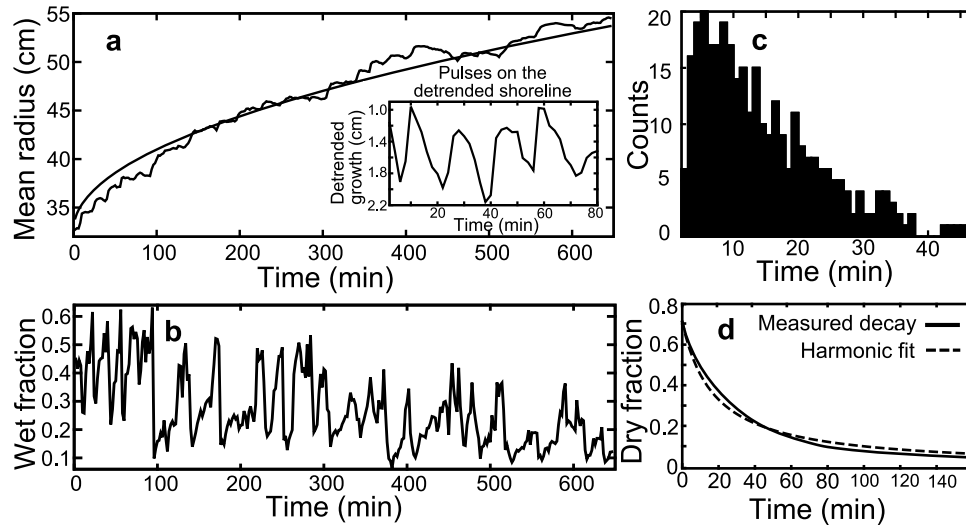


**Figure 9.** Various measures of the avulsion timescale, calculated for R20. (a) Because the initial channelization phase of the avulsion sequence strongly progrades the shoreline, pulses superimposed on the mean fan margin growth correspond to the avulsion timescale, because of the early phase of abrupt channelization and lobe establishment. Pictured in the inset of Figure 9a is an 80 min segment of the mean radial growth, detrended to show the fluctuations around the mean that correspond to avulsions. (b) The fraction of the fan covered by water also fluctuates with the avulsion timescale, as the system alternately floods and channelizes. (c) The bulk channel decorrelation timescale, which gives a distribution of time lapses for wetted pixels to become dry. (d) A measurement of the average decay of cumulative dry fraction, as dry portions of the fan are progressively visited by the flow. The dry fraction decay is well approximated with a harmonic decay fit (4) with an internal timescale of 18 min. While power law with exponent 0.29 can also be used to describe the increasing cumulative inundation, the harmonic decay function provides a more parsimonious description, as it uses only the single parameter of the avulsion timescale itself. The various measures of avulsion time are consistent.

the sediment flux by dividing it by our estimated porosity and lessening it by the volume lost as the coarse grains prograde at the measured angle over the fine-grain deposit, we calculate  $r(t) = 5.75t^{1/3}$ . A direct fit of our data with the expected exponent of  $1/3$  returns a coefficient of 5.53, with  $R^2 = 0.96$ . The correspondence of the expected and observed coefficients verifies that our experimental fans' bulk behavior can be well described with cone geometry; it also provides support for our porosity estimate and the assumption of a linear fan profile.

[44] As discussed, our channels were likely in a transitional regime between laminar and turbulent flow (Table 2). An appropriate critical Shields stress for our grains could lie anywhere within the range of observed values,  $\tau_c^* \sim 0.05$ – $0.3$  [Yalin and Karahan, 1979; Buffington and Montgomery, 1997; Lobkovsky *et al.*, 2007]. Our estimated Shields stress values of  $\sim 0.3$  (Table 2, column (i)) might indicate that our experimental fans are organized to slopes near critical. Though we cannot say conclusively whether our fans are organized to this type of critical slope, the consistency of bulk measured slopes within and across our runs allows us to state that the system did organize to some particular equilibrium slope. That the slope did not vary between runs, though the (coarse grain) feed rate varied by a factor of four, conflicts with equilibrium channel theory, and suggests that the slope must have been set by factors that were constant across runs: namely, the water flux and the sediment type.

#### 4.4. Avulsion Process and Timescale

[45] To measure the avulsion timescale in our experiments, we used the four methods described in Section 3.3. First, we examined the frequency of pulses superimposed on the mean fan margin growth trend. We observed that these pulses were periodic, but with a period that increased with time through the experiment, as we hypothesized (Figure 9a). We measured these periodicities by running autocorrelations on detrended segments of the pulsing fan margin. These timescales ranged from  $\sim 20$ – $25$  min for R20, for times in the experiment from  $\sim 100$ – $500$  min. Similarly, we measured the frequency of fluctuations in the fan wet fraction (Figure 9b), and this measurement also yielded timescales of approximately 20–25 min. Our measurement of the channel decorrelation timescale gave a distribution of times with typical values of 10–15 min, or, approximately half the avulsion timescale, which is what we would expect from such a measurement (Figure 9c). Finally, we measured the average decay of the dry fraction on the fan, and fit it with a harmonic function of the form below, after Cazanagli *et al.* [2002]:

$$f_{dry}(t) = \frac{f_{dry,0}}{1 + \frac{t}{T_A}} \quad (4)$$

where  $f_{dry}(t)$  is the average decay of the dry fraction with time,  $f_{dry,0}$  is the initial dry fraction, and  $T_A$  is the avulsion timescale. Cazanagli *et al.* [2002] described the time constant in the decay as a landscape reworking time, related to how

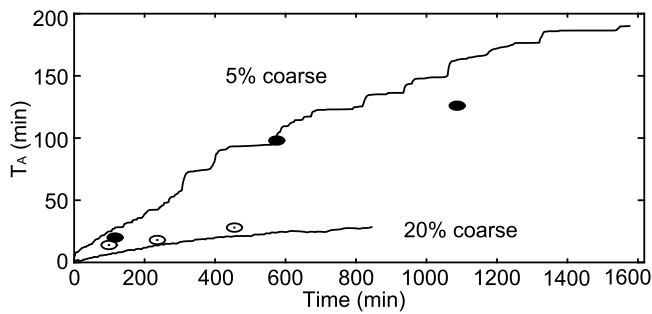


**Figure 10.** Measured avulsion timescales obtained from autocorrelations of detrended shoreline pulses are seen to increase through time and to be longer for lower sediment feed rate (solid and open dots for R5 and R20). The avulsion timescales predicted from the formulation (6) proposed in the Discussion for R5 (upper line) and R20 (lower line) through time are consistent with measurements.

long it takes to eventually activate the entire fan surface, and conjectured that this may be representative of the time it takes to fill a channel. We find agreement with this idea, in that the  $T_A$  resulting from our fit (Figure 9d) is 18 min, and consistent with our other measurements of the avulsion timescale.

[46] Using the shoreline pulse method we measured three separate avulsion timescales for each experiment to assess variations in the coarse fan  $T_A$  with coarse feed rate through time. For this analysis, we segmented the detrended shoreline to portions of four pulses each, measured the peak of the autocorrelation of each segment, and plotted the measured peak in the middle of the segment. We confirm our hypothesis that the avulsion timescale increases with time for both R5 and R20, and that avulsion timescales are longer for the lower coarse sediment feed rate of R5 (Figure 10).

## 5. Discussion

### 5.1. Reoccupation and Fan Margin Growth

[47] Our formulation of the growth of lobe radius of curvature with fan radius worked well to describe the manner in which reoccupying channels widened their lobes. Lobe radius of curvature is of particular interest in our slope-driven framework because it is closely linked to the distraintment slope, and according to our formulation, the center of this radius of curvature marks the hinge point from which this slope is established. Though we could not resolve the height of this hinge point with our topographic data and therefore infer distraintment slope values in our experiment, our formulation of  $R(r)$  can be taken as a first step toward making this quantification in future studies.

### 5.2. Channels and Threshold Slopes

[48] *Threshold channel geometry.* In the previous section, we showed that our channel dimensions are similar to those expected for threshold-organized canals, and in conflict with the equilibrium channel geometry predictions. These channel geometry predictions from Parker [1978] would not however be likely to apply in this case because they make use of flow resistance and sediment transport relations calibrated specifically from the wide gravel bedded streams for

which the Parker framework is designed, which are not justifiably transferrable to our experimental channels, where we might expect different relationships. Because our channels were self-formed by material moving as bed load, we would however expect that a gravel bedded stream could be an appropriate natural analogue. The distinguishing characteristic that we propose sets the geometries of our channels is that these bypass channels are not in equilibrium with the high flux of incoming sediment, and can therefore be organized to a threshold grain entrainment stress.

[49] The correspondence between our measured channel dimensions and the canal geometry predictions supports our idea that the upper reaches of our fans are acting as sediment bypass systems with a slope corresponding to a grain entrainment stress, while the grains distraint at a lower slope at the foot of the channel and progressively backfill. Our channels likely present an end-member case, in that their entrainment and distraintment reaches are so distinct; this may be due to a higher initial momentum of grains entering the experimental system, or to the steep slope set by our coarse, heavy grains. However, some reach separation effect should be generally present in all recursively avulsing systems, though perhaps not as clearly expressed. Results from other experimental fan studies support this separation; *Sheets et al.* [2002] for example measured an inverse relation between flow occupation and effective rates of aggradation. Their results demonstrated that the upstream portions of channels exhibited little to no deposition – i.e., they acted as bypass reaches. In nature, steep, coarse-grained alluvial fans on which inertia and gravity effects can be strong might also be expected to express a detectable separation between zones of entrainment and distraintment. The *Stock et al.* [2008] study of alluvial fans found that the upper portions of fans show both linear profiles and a lack of the grain size trends expected from downstream fining effects, consistent with sediment bypass as a possible interpretation. An important distinction for translating our results to real fans is that in nature, flow on fans is intermittent, and when the flow drops, grains can cease transport to deposit in the upper bypass zones. According to our hypotheses this deposition would however be generally temporary: at this established entrainment slope, the position of a grain sitting atop the channel bed is unstable, because it is above entrainment threshold for bankfull flood. It interferes with the threshold channel geometry, which will be re-established once the flow reaches flood levels again.

[50] The consideration of separate entrainment and distraintment conditions, and of ‘bypass reaches’ connecting the inlet to the moving distraintment boundary, may be a key, unexplored dynamic of channels in depositional systems.

[51] *Controls on bulk slope.* Because the *Savenije* [2003] equations depend only on bed load grain type and water flux, not on sediment flux, they predict approximately the same channel geometries for both of our runs, and this is what we see, despite a factor of four change in coarse sediment supply. If bulk fan slope is also set by either the entrainment or distraintment of grains, we would expect the threshold criterion to result in a fairly constant slope between runs, which it is. This observation is in contrast with the *Parker et al.* [1998a] model, which predicts a slope proportional to the sediment flux, and with other studies that have documented bed load channel slope dependence on sediment

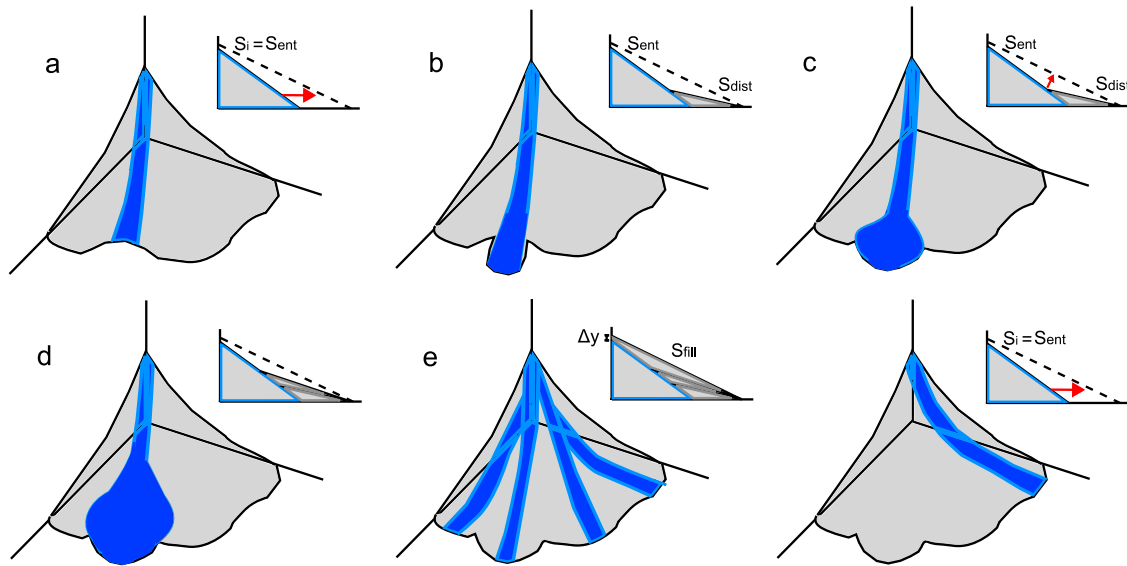


**Figure 11.** Schematic of the avulsion sequence, as related to slope fluctuations. Compare with images of experimental avulsion sequence, in corresponding panels of Figure 4a–4f. (a) A channel is initially cut down to entrainment conditions, setting a within-channel slope ( $S_{ent}$ ) corresponding to a grain entrainment stress. (b) As the channel-volume of excavated grains, in addition to the constant sediment influx, runs out at the end of the channel, the shoreline advances and lowers the within-channel slope at the shoreline to a distraintment value ( $S_{dist}$ ), below which grains cannot be transported. (c) Unable to prograde further, the channel first flares to set the local shoreline to the distraintment slope, thereby establishing the semicircular lobe geometry. (d) The channel now begins to fill in the wedge of space between the entrainment and distraintment slopes. Because grains bypass the upper entrainment reaches and are stopped only upon encountering the earlier deposits toward the shoreline, deposition progresses from the toe of the channel upstream, in a manner reminiscent of upslope-migrating stopping fronts in dry granular piles. (e) This stopping-up of the grains allows for the gradual build up to a higher slope value ( $S_{fill}$ ) that connects the new shoreline to the apex, as the channel is filled with sediment. The fan now floods to search for a new path. Because the  $S_{ent}$  threshold required to cut a new channel has not been exceeded, a new channel cannot now be initiated here; however, by the time flow returns to this part of the fan, the slow aggradation of the apex (Figure 12a) will have oversteepened it again. (f) A new channel is cut and the cycle repeats.

flux [e.g., Bagnold, 1986; Parker *et al.*, 1998b]. The Parker *et al.* [1998a] sediment extraction model also predicts a concave profile, whereas the linear profiles observed in our experiments support the hypothesis that the fan acts as a sediment bypass zone. We interpret that the observed disconnect of bulk slope from the imposed sediment load in our experiments is a result of our channels not being in equilibrium with the supplied load, and we expect that this non-equilibrium condition is an effect that will be present to some degree on all fans that form at slope breaks; we will explore this topic further in a future paper.

### 5.3. Avulsion Process and Timescale

[52] *Avulsion process.* We propose an analogy between the avulsion sequence and the intermittent avalanches of granular piles, which supplies a simple explanation for the separation between entrainment and distraintment reaches suggested by our threshold channels. When a channel is cut (Figure 11a), a channel-volume layer of grains is mobilized, to deposit out at the mouth of the channel (Figure 11b). Deposition at the fan margin first locally flares out to set the fan outlet geometry to the low distraintment slope associated with the canal-geometry channel width and depth. Because lobe shape here is controlled by the distraintment slope with

respect to a hinge point within the channel, lobe geometry becomes locally circular (Figure 11c). Grains still being fed into the system ‘backfill’, and the depocenter progresses from the fan margin back up the fan (Figure 11d). This dynamic is similar to the ‘stopping front’ that migrates upslope in a granular avalanche [Rajchenbach, 1990], where avalanching grains stop moving because pocket geometry creates too high a friction angle to be overcome by the momentum that was reduced by the slope break. Grains in water cease transport for the same reason, with the difference that an additional fluid drag component to the momentum results in a lower fan system slope. The deposition is then accelerated by the increase in flow width at the lobe. This backfilling fills a wedge of space, the lower angle of which was set by the lowest distraintment slope; the upper angle connects the fan margin to the fan apex, as the channel fills with sediment. The abrupt increase in within-channel slope when a channel is cut, followed by gradual backfilling, results in asymmetric slope fluctuations on the fan, similar to those observed for dry avalanches (Figure 8 inset). The ~10% magnitude of our estimated bulk slope fluctuations is comparable to the 5–15% magnitude of slope fluctuations in dry granular avalanching systems [e.g., Jaeger *et al.*, 1989; Evesque *et al.*, 1993].



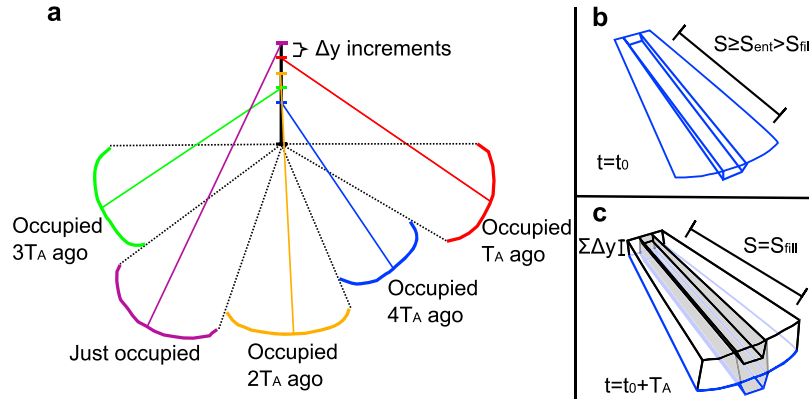


**Figure 12.** (a) Sketch of channel region slope elevations, pictured for a fan with channel reoccupation to illustrate the  $\Sigma\Delta y$  concept. Each solid line from the shore to the apex represents the  $S_{fill}$  reached the last time the region was active. Regions without recent activity have slopes from the apex height to the shoreline that are greater than  $S_{fill}$ , because the apex has meanwhile been aggrading. (b) A channel is initially cut into the sitting floodplain of an oversteepened region. (c) At the end of the channel activation,  $T_A$  later, the region has filled with sediment, such that the slope from the shoreline to the apex is now  $S_{fill}$ . This enclosed volume geometrically specifies the avulsion timescale, given an incoming sediment flux. Further, for systems with separable coarse and fine grain populations, the shaded volume representing the channel which has cut, aggraded, and filled (and possibly meandered side-to-side) is filled by coarse grains, while the remaining white volume is filled by fine grains via floodplain sedimentation.

[53] For channels formed by incision, as on our experimental fans, the channelization process requires a slope such that flow is strong enough to entrain grains from the fan deposit, which we term the entrainment slope  $S_{ent}$ , analogous to the static angle of repose (Figures 11a and 11f). If no portion of the fan presents a steep enough path ( $S \geq S_{ent}$ ) to focus flow into a new channel, the fan will deposit via unconfined flow until the threshold is crossed. We define  $\Delta y$  (Figure 11e) to be the additional height due to vertical aggradation at the apex during the time of one avulsion sequence, resulting from the requirement that the apex build until the entrainment threshold is crossed somewhere before rechannelizing. Note that  $\Delta y$  is not an independently introduced term, but a simple geometric consequence of our entrainment and distraintment threshold slope criteria. Because the slope to which a channel fills ( $S_{fill}$ ) is lower than  $S_{ent}$ , the fan cannot immediately rechannelize in that location. That the value of  $S_{fill}$  lies between  $S_{ent}$  and  $S_{dist}$  can be seen from the within-channel slope profiles of Figure 11: since  $\Delta y$  at the apex maintains the equilibrium slope with respect to the mean fan radius, not to the individual active lobe, it does not increase the apex height enough compared to the localized radial increase to make  $S_{fill}$  parallel to  $S_{ent}$ . If, after filling a given channel, the flow subsequently executes 3–4 avulsions elsewhere, it will however have elevated the apex by 3–4 multiples of  $\Delta y$  (Figure 12a), and may then be sufficiently oversteepened to rechannelize there. This  $S \geq S_{ent}$  threshold requirement therefore dictates a timescale over which previous channels do act as topographic repellers [c.f., *Leeder*, 1978; *Allen*, 1978]; it is only beyond this timescale that other mechanisms can induce channel reoccupation.

[54] Note that reoccupation is not required for this framework; the oversteepening condition could result from an apex elevation that exceeds the critical limit on average, but is not uniform over the newly channelized region, as it is when overlying a former occupation. This steepening at the apex

with respect to a given region will be a logical result of time periods of depositional activity elsewhere on the fan in any scenario for which activity is not uniform over the fan through time; i.e., for any channelized fan system. Figure 13 shows the more generic case that does not include incidences of channel reoccupation, though reoccupation is still implied in Figure 12 because this simplification helps to illustrate the oversteepening point.

[55] If placed the context of granular avalanches, the self-organizing channel geometry would be the regulatory mechanism that causes the avulsion sequence to be one of the neatly periodic (Figure 9a) cases of granular avalanching.

[56] *Avulsion timescale.* The timescale of channel avulsion can be estimated in terms of the volume to be filled with sediment, divided by the rate at which sediment enters the system. In this section, we delineate the volume to be filled within an avulsion timescale, as a geometric consequence of our slope-controlled understanding of avulsion.

[57] This volume is determined by the size of a channel, and by the region of surrounding floodplain influenced by the channel, roughly defined by the angular size of the channel's lobe at the shoreline (Figures 12c and 13c). This volume is filled as bed load deposition within a channel, floodplain deposition in the area around the channel, and by lateral channel migration, which deposits bed load over a broader area.

[58] We consider the avulsion timescale  $T_A$  proposed in *Reitz et al.* [2010], in which the volume for  $T_A$  is the product of the mean fan margin position  $r(t)$ , channel depth ( $h$ ), and average wetted width ( $B_{eff}$ ), and sediment is fed at rate  $Q_s$ :

$$T_A(t) = \frac{hB_{eff}r(t)}{Q_s} \quad (5)$$

However, we modify this timescale to include the angle subtended by a typical channel lobe ( $\theta$ ) and to eliminate the

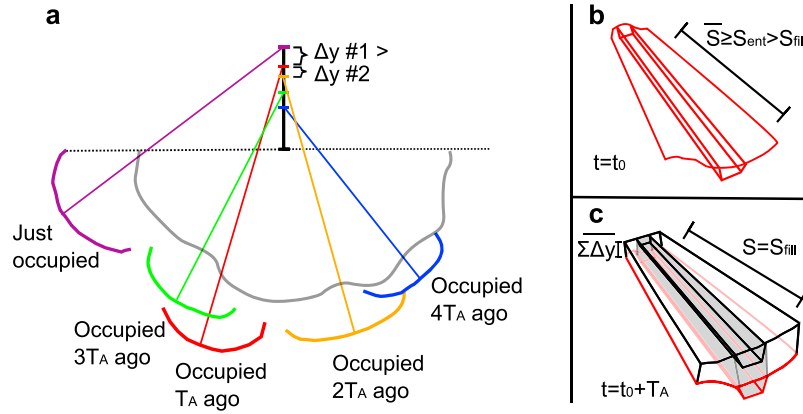


**Figure 13.** A sketch similar to Figure 12, but with the reoccupation assumption relaxed. (a) Channel regional slope elevations. (b) Initial channel cut into uneven region. (c) Channel region filled to slope of  $S_{fill}$ . The height of aggradation over a newly channelized region is not now uniform, so the  $\Sigma\Delta y$  of (6) to be aggraded before the next avulsion represents an average over the region. Although individual increments of  $\Delta y$  are not deterministically predictable without deterministic reoccupation, the requirement that a fan be radially smooth to first order leads to  $\Sigma\Delta y$  values that are on average the same as in Figure 12.

necessity of the effective channel width correction. We also include an additional term,  $\Sigma\Delta y$ , to represent the total amount of vertical aggradation at the fan apex since the region was last depositionally active, which marks out the average height to which deposition must aggrade over the angular area of the region (Figure 12c). We propose:

$$T_A(t) = \left[ hBr(t) + \frac{\theta}{2\pi} \frac{\pi}{3} \Sigma\Delta y r^2(t) \right] Q_s^{-1},$$

or, simplified,

$$T_A(t) = \left[ hBr(t) + \frac{\theta}{6} \Sigma\Delta y r^2(t) \right] Q_s^{-1}, \quad (6)$$

which marks out the available volume to be filled prior to avulsion and divides this by the sediment flux. This formulation neglects both the initially incised channel-volume of sediment and the volume of sediment comprising the distrainment lobe at the end of the channel, under the assumption that the latter is largely composed of the former, such that the two volumes cancel (seemingly valid for our experiments at least). It also assumes that any change in  $S_{fill}$  from one period of activity to the next is negligible, an assumption supported by the consistency of bulk measured slopes in our runs through time after the avulsion cycle is established (Figure 8).

[59] The left-hand term of (6) corresponds to the channel-filling timescale proposed in Reitz *et al.* [2010]. The right-hand term represents the additional space-filling that must occur to fill in the angular region, through either channel movement or overbank sedimentation. In natural systems in which channels are cut deeply and are not very mobile, we expect the channel-filling term on the left to be dominant, and the term on the right to represent floodplain sedimentation; this dominance of the channel-filling term explains the convergence of natural measured avulsion timescales to the channel-filling timescale proposed in Reitz *et al.* [2010]. For shallower, more mobile channels, we would expect the right-hand term to play a larger role.

[60] Although (6) is developed for the volume of a section of a cone, which is appropriate for our experimental fans and

for steep, straight-profile alluvial fans, it would be straightforward to adjust the framework for an arbitrary fan volume, such as one with a diffusive, concave slope. Also, though it would seem that  $S_{ent}$  and  $S_{dist}$  have dropped out of the formulation, they are still present in setting  $\Sigma\Delta y$  and determining channel geometry. A better quantification of  $S_{ent}$  and  $S_{dist}$  as they relate to grain characteristics and water momentum will allow us to improve on this framework. We expect that both  $S_{ent}$  and  $S_{dist}$  will show a dependence on water flux. Indeed, preliminary results from studies at the University of Texas at Austin indicate that the avulsion timescale varies with water flux as well as sediment flux, and they attribute the dependence on water flux to its effect on lobe runout length, which would be directly related to  $S_{dist}$  [Powell *et al.*, 2010].

[61] Note that the only assumption used to generate (6) is the separation between entrainment and distrainment slopes.

[62] *Testing against experiments.* Here we compare the geometric avulsion timescale prediction of (6) with our experimental avulsion data. Figure 10 plots the avulsion timescale of (6) as a function of time, growing with  $r(t)$ , for R5 and R20. We use  $\theta \sim \pi/5$  ( $36^\circ$ ) and the values of  $h$  and  $B$  reported in Table 1. Again  $Q_s$  is divided by the porosity and lessened by the volume lost as the coarse fan progrades over the fine-grained deposit. Though our measurements were not taken with the  $\Sigma\Delta y$  parameter in mind, we estimate its value as follows: for a final fan deposit of 9.9 cm height at the apex, divided by 844 min runtime for an aggradation rate, multiplied by  $\sim 20$  min avulsion timescale to get amount of aggradation per channel lifetime, and multiplied by 5 for the average number of channels, we estimate  $\Sigma\Delta y$  to be  $\sim 1.17$  cm. That this  $\Sigma\Delta y$  term is comparable to our channel depth is not likely coincidental, and is consistent with other studies in which channel depth emerges as a fundamental length scale governing fan deposition dynamics in both experiments and natural systems [Sheets *et al.*, 2002; Jerolmack and Mohrig, 2007; Straub *et al.*, 2009]. For both R5 and R20, we find agreement between measured and predicted avulsion timescales. Because the proposed timescale

of (6) is driven simply by mass conservation on a bulk scale, we expect that it can be extended from experiments to nature.

## 6. Conclusion

[63] In this paper, we have presented a new framework for the understanding of avulsion mechanics, and we have directly tested aspects of this framework with our experiments. Our formulation follows from the assumption that (1) the channel-forming requirement that a critical slope to entrain grains from the bed be exceeded and the corresponding organization of specific packed channel bed geometries and (2) the momentum carried by grains entering at the fan inlet result in a slope separation corresponding to separate conditions of grain entrainment and distrainment. Drawing from this slope separation hypothesis, we offer a new solution to the canal paradox for out-of-equilibrium channels, and present an avulsion timescale prediction from a formulation of the volume of space to be filled between avulsions.

[64] Aspects of our framework that we support with data from our experimental fans are the threshold channel predictions, the slope invariance with sediment supply, and the increase of avulsion timescale with time and decrease in timescale with sediment feed rate. Though our data support the framework of a slope separation driven by separate entrainment and distrainment conditions, it was not feasible for us to directly measure the slope distinction in our experiments, so final confirmation will be a subject for future research. The determination of the distrainment slope as a function of grain type, bed packing and incoming grain momentum, and the calculation of the difference between distrainment and entrainment slopes for different types of sediment, are open, interesting questions with a wide range of implications for alluvial channels of all types. Further, the discrepancy between entrainment and distrainment conditions in general has intriguing implications for bed load transport in any system with spatially or temporally varying depositional patterns.

## Appendix A: Shoreline Geometry Evolution

[65] Below we trace the intermediate steps for arriving at (2). The aim is an equation for the evolution of lobe radius of curvature  $R$  with fan radius  $r$ , given initial  $R_0$  and  $r_0$ , and given the opening angle  $\theta$ . We can solve for this with simple geometric and algebraic manipulations; see Figure 6b for a sketch of relevant variables, and note that in the below steps,  $u$ ,  $v$ ,  $w$ ,  $x$ ,  $y$ ,  $z$ , and  $\alpha$  are not new variables, but stand-ins to clarify the steps.

$$\begin{aligned} x &= r - r_0 \\ w &= (r_0 - R_0)\cos\theta \\ z &= (r_0 - R_0)\sin\theta \\ v &= \sqrt{R_0^2 - z^2} \\ y &= w + v + x \\ u &= \sqrt{r^2 + y^2 - 2ry\cos\theta} \\ \alpha &= \sin^{-1}\left(\frac{y\sin\theta}{u}\right) \\ R &= \frac{u}{2\cos\alpha} \end{aligned}$$

These steps yield (2), an equation for the evolution of lobe radius of curvature  $R$ , as the consequence of the stated geometric constraints.

## Notation

$S_{ent}$	slope associated with organization to a grain entrainment stress
$S_{dist}$	slope associated with organization to a grain distrainment stress
$S_{fill}$	slope connecting edge of lobe at shoreline with fan apex
$h$	channel depth
$B$	channel width
$\phi$	angle of repose of coarse sediment
$Q_w$	water flux
$u$	average bankfull within-channel flow velocity
$r$	average fan radius
$t$	time
$Q_s$	sediment flux
$S$	average fan slope
$\tau_c^*$	critical Shields stress for initiation of motion
$f_{dry}$	average decay of the dry fraction with time
$f_{dry,0}$	initial dry fraction
$T_A$	mean time period between successive avulsions
$R$	lobe radius of curvature
$R_0$	initial lobe radius of curvature
$r_0$	initial average fan radius
$\theta$	angle subtended by a channel lobe
$B_{eff}$	effective channel width
$\Delta y$	height aggraded at fan apex through the time period of one $T_A$
$\Sigma\Delta y$	total height aggraded at apex since a newly channelized region was last active

[66] **Acknowledgments.** We thank Emily Moberg for assistance with experiments; Olivier Devauchelle, Wonsuck Kim, John Swenson and Elsa Bayart for useful discussions; and Raleigh Martin for assistance with figures. We gratefully acknowledge NSF grant EAR-0746138 to Douglas J. Jerolmack. We thank Jonathan Stock, Andrew Nicholas, and an anonymous reviewer for their helpful suggestions, which improved the manuscript significantly.

## References

- Aalto, R., J. Lauer, and W. Dietrich (2008), Spatial and temporal dynamics of sediment accumulation and exchange along Strickland River floodplains (Papua New Guinea) over decadal-to-centennial timescales, *J. Geophys. Res.*, *113*, F01S04, doi:10.1029/2006JF000627.
- Allen, J. R. L. (1978), Studies in fluvial sedimentation: An exploratory quantitative model for the architecture of avulsion-controlled alluvial suites, *Sediment. Geol.*, *21*, 129–147.
- Altshuler, E., O. Ramos, C. Martinez, L. E. Flores, and C. Noda (2001), Avalanches in one-dimensional piles with different types of bases, *Phys. Rev. Lett.*, *86*, 5490–5493, doi:10.1103/PhysRevLett.86.5490.
- Anczy, C., F. Bigillon, P. Frey, J. Lanier, and R. Ducret (2002), Saltating motion of a bead in a rapid water stream, *Phys. Rev. E*, *66*, 036306, doi:10.1103/PhysRevE.66.036306.
- Ashworth, P., J. Best, and M. Jones (2004), Relationship between sediment supply and avulsion frequency in braided rivers, *Geology*, *32*, 21–24, doi:10.1130/G19919.1.
- Aslan, A., W. Autin, and M. Blum (2005), Causes of river avulsion: Insights from the late Holocene avulsion history of the Mississippi River, USA, *J. Sediment. Res.*, *75*, 650–664, doi:10.2110/jsr.2005.053.
- Bagnold, R. A. (1980), An empirical correlation of bedload transport rates in flumes and natural rivers, *Proc. R. Soc. London, Ser. A*, *372*, 453–473, doi:10.1098/rspa.1980.0122.

- Bagnold, R. A. (1986), Transport of solids by natural water flow: Evidence for a worldwide correlation, *Proc. R. Soc. London, Ser. A*, 405, 369–374, doi:10.1098/rspa.1986.0059.
- Bak, P., C. Tang, and K. Wiesenfeld (1987), Self-organized criticality: An explanation of  $1/f$  noise, *Phys. Rev. Lett.*, 59, 381–384, doi:10.1103/PhysRevLett.59.381.
- Beaumont, P., and T. M. Oberlander (1971), Observations on stream discharge and competence at Mosaic Canyon, Death Valley, California, *Geol. Soc. Am. Bull.*, 82, 1695–1698, doi:10.1130/0016-7606(1971)82[1695:OOSDAC]2.0.CO;2.
- Brizga, S., and B. Finlayson (1990), Channel avulsion and river metamorphosis: The case of the Thomson River, Victoria, Australia, *Earth Surf. Processes Landforms*, 15, 391–404, doi:10.1002/esp.3290150503.
- Bryant, M., P. Falk, and C. Paola (1995), Experimental study of avulsion frequency and rate of deposition, *Geology*, 23, 365–368, doi:10.1130/0091-7613(1995)023<0365:ESOFA>2.3.CO;2.
- Buchholz, V., and T. Pöschel (1994), Numerical investigations of the evolution of sandpiles, *Physica A*, 202, 390–401, doi:10.1016/0378-4371(94)90467-7.
- Buffington, J. M., and D. R. Montgomery (1997), A systematic analysis of eight decades of incipient motion studies, with special reference to gravel-bedded rivers, *Water Resour. Res.*, 33, 1993–2029, doi:10.1029/96WR03190.
- Cazanacli, D., C. Paola, and G. Parker (2002), Experimental steep, braided flow: Application to flooding risk on fans, *J. Hydraul. Eng.*, 128, 322–330, doi:10.1061/(ASCE)0733-9429(2002)128:3(322).
- Clarke, L., T. Quine, and A. Nicholas (2010), An experimental investigation of autogenic behaviour during alluvial fan evolution, *Geomorphology*, 115, 278–285, doi:10.1016/j.geomorph.2009.06.033.
- Dade, W. B., and P. Friend (1998), Grain-size, sediment-transport regime, and channel slope in alluvial rivers, *J. Geol.*, 106, 661–676, doi:10.1086/516052.
- Daerr, A., and S. Douady (1999), Two types of avalanche behaviour in granular media, *Nature*, 399, 241–243, doi:10.1038/20392.
- Devauchelle, O., A. Petroff, A. Lobkovsky, and D. Rothman (2011), Longitudinal profile of channels cut by springs, *J. Fluid Mech.*, 667, 38–47, doi:10.1017/S0022112010005264.
- Díaz, J., A. Fowler, A. Muñoz, and E. Schiavi (2008), Mathematical analysis of a model of river channel formation, *Pure Appl. Geophys.*, 165, 1663–1682, doi:10.1007/s00024-004-0394-3.
- Eaton, B., M. Church, and R. Millar (2004), Rational regime model of alluvial channel morphology and response, *Earth Surf. Processes Landforms*, 29, 511–529, doi:10.1002/esp.1062.
- Edmonds, D., D. Hoyal, B. Sheets, and R. Slingerland (2009), Predicting delta avulsions: Implications for coastal wetland restoration, *Geology*, 37, 759–762, doi:10.1130/G25743A.1.
- Evesque, P., D. Fargeix, P. Habib, M. P. Luong, and P. Porion (1993), Pile density is a control parameter of sand avalanches, *Phys. Rev. E*, 47, 2326–2332, doi:10.1103/PhysRevE.47.2326.
- Ferguson, R. I., and M. Church (2004), A simple universal equation for grain settling velocity, *J. Sediment. Res.*, 74, 933–937, doi:10.1306/051204740933.
- Frette, V., K. Christensen, A. Malthé-Sørensen, J. Feder, T. Jøssang, and P. Meakin (1996), Avalanche dynamics in a pile of rice, *Nature*, 379, 49–52, doi:10.1038/379049a0.
- Goedhart, M., and N. Smith (1998), Braided stream aggradation on an alluvial fan margin: Emerald Lake fan, *Can. J. Earth Sci.*, 35(5), 534–545, doi:10.1139/e97-128.
- Grumbacher, S., K. McEwen, D. Halverson, and D. Jacobs (1993), Self-organized criticality: An experiment with sandpiles, *Am. J. Phys.*, 61, 329–335, doi:10.1119/1.17264.
- Held, G. A., D. H. Solina II, D. T. Keane, W. J. Haag, P. M. Horn, and G. Grinstein (1990), Experimental study of critical-mass fluctuations in an evolving sandpile, *Phys. Rev. Lett.*, 65, 1120–1123, doi:10.1103/PhysRevLett.65.1120.
- Hirano, M. (1973), River-bed variation with bank erosion, *Proc. Jpn. Soc. Civ. Eng.*, 1973, 13–20, doi:10.2208/jscej1969.1973.210.13.
- Hooke, R., and R. Dorn (1992), Segmentation of alluvial fans in Death Valley, California: New insights from surface exposure dating and laboratory modelling, *Earth Surf. Processes Landforms*, 17, 557–574, doi:10.1002/esp.3290170603.
- Hoyal, D. C. J. D., and B. A. Sheets (2009), Morphodynamic evolution of experimental cohesive deltas, *J. Geophys. Res.*, 114, F02009, doi:10.1029/2007JF000882.
- Jaeger, H., C. Liu, and S. Nagel (1989), Relaxation at the angle of repose, *Phys. Rev. Lett.*, 62(1), 40–43, doi:10.1103/PhysRevLett.62.40.
- Jain, V., and R. Sinha (2003), Hyperavulsive-anabranching Bagmati river system, north Bihar plains, eastern India, *Z. Geomorphol.*, 47, 101–116.
- Jerolmack, D. J., and D. Mohrig (2007), Conditions for branching in depositional rivers, *Geology*, 35, 463–466, doi:10.1130/G23308A.1.
- Jerolmack, D. J., and C. Paola (2007), Complexity in a cellular model of river avulsion, *Geomorphology*, 91, 259–270, doi:10.1016/j.geomorph.2007.04.022.
- Kim, W., and D. J. Jerolmack (2008), The pulse of calm fan deltas, *J. Geol.*, 116, 315–330, doi:10.1086/588830.
- Kim, W., C. Paola, J. B. Swenson, and V. R. Voller (2006a), Shoreline response to autogenic processes of sediment storage and release in the fluvial system, *J. Geophys. Res.*, 111, F04013, doi:10.1029/2006JF000470.
- Kim, W., C. Paola, V. R. Voller, and J. B. Swenson (2006b), Experimental measurement of the relative importance of controls on shoreline migration, *J. Sediment. Res.*, 76, 270–283, doi:10.2110/jsr.2006b.019.
- Kodoma, Y. (1994), Downstream changes in the lithology and grain size of fluvial gravels, the Watarase River, Japan: Evidence of the role of abrasion in downstream fining, *J. Sediment. Res.*, A64, 68–75.
- Lajeunesse, E., L. Malverti, P. Lancien, L. Armstrong, F. Métivier, S. Coleman, C. E. Smith, T. Davies, A. Cantelli, and G. Parker (2010a), Fluvial and submarine morphodynamics of laminar and near-laminar flows: A synthesis, *Sedimentology*, 57, 1–26, doi:10.1111/j.1365-3091.2009.01109.x.
- Lajeunesse, E., L. Malverti, and F. Charru (2010b), Bed load transport in turbulent flow at the grain scale: Experiments and modeling, *J. Geophys. Res.*, 115, F04001, doi:10.1029/2009JF001628.
- Leeder, M. (1978), A quantitative stratigraphic model for alluvium, with special reference to channel deposit density and interconnectedness, *Fluv. Fluvial Sediment.*, 5, 587–596.
- Lobkovsky, A. E., B. E. Smith, A. Kudrolli, D. Mohrig, and D. H. Rothman (2007), Erosive dynamics of channels incised by subsurface waterflow, *J. Geophys. Res.*, 112, F03S12, doi:10.1029/2006JF000517.
- Malverti, L., E. Lajeunesse, and F. Métivier (2008), Small is beautiful: Upscaling from microscale laminar to natural turbulent rivers, *J. Geophys. Res.*, 113, F04004, doi:10.1029/2007JF000974.
- Martin, J., B. Sheets, C. Paola, and D. Hoyal (2009), Influence of steady base-level rise on channel mobility, shoreline migration, and scaling properties of a cohesive experimental delta, *J. Geophys. Res.*, 114, F03017, doi:10.1029/2008JF001142.
- Mohrig, D., P. Heller, C. Paola, and W. Lyons (2000), Interpreting avulsion process from ancient alluvial sequences: Guadalupe-Matarranya system (northern Spain) and Wasatch Formation (western Colorado), *Geol. Soc. Am. Bull.*, 112, 1787–1803, doi:10.1130/0016-7606(2000)112<1787:IAPFAA>2.0.CO;2.
- Neill, C., and L. Deegan (1986), The effect of Mississippi River delta lobe development on the habit composition and diversity of Louisiana coastal wetlands, *Am. Midl. Nat.*, 116, 296–303, doi:10.2307/2425737.
- Nicholas, A. P., L. Clarke, and T. A. Quine (2009), A numerical modelling and experimental study of flow width dynamics on alluvial fans, *Earth Surf. Processes Landforms*, 34, 1985–1993, doi:10.1002/esp.1839.
- Paola, C., K. Straub, D. Mohrig, and L. Reinhardt (2009), The “unreasonable effectiveness” of stratigraphic and geomorphic experiments, *Earth Sci. Rev.*, 97, 1–43, doi:10.1016/j.earscirev.2009.05.003.
- Parker, G. (1978), Self-formed straight rivers with equilibrium banks and mobile bed. Part 2. The gravel river, *J. Fluid Mech.*, 89, 127–146, doi:10.1017/S0022112078002505.
- Parker, G., C. Paola, K. Whipple, and D. Mohrig (1998a), Alluvial fans formed by channelized fluvial and sheet flow. I: Theory, *J. Hydraul. Eng.*, 124, 985–995, doi:10.1061/(ASCE)0733-9429(1998)124:10(985).
- Parker, G., C. Paola, K. Whipple, D. Mohrig, C. M. Toro-Escobar, M. Halverson, and T. W. Skoglund (1998b), Alluvial fans formed by channelized fluvial and sheet flow. II: Application, *J. Hydraul. Eng.*, 124, 996–1004, doi:10.1061/(ASCE)0733-9429(1998)124:10(996).
- Peakall, J., P. Ashworth, and J. Best (1996), Physical modelling in fluvial geomorphology: Principles, applications, and unresolved issues, in *The Scientific Nature of Geomorphology: Proceedings of the 27th Binghamton Symposium in Geomorphology held 27–29*, edited by B. L. Rhoads and C. E. Thorn, pp. 221–253, John Wiley, New York.
- Pizzuto, J. (1987), Sediment diffusion during overbank flows, *Sedimentology*, 34, 301–317, doi:10.1111/j.1365-3091.1987.tb00779.x.
- Powell, E., W. Kim, and T. Muto (2010), Quantifying the fluvial autogenic processes: Tank Experiments, Abstract EP43F-03 presented at 2010 Fall Meeting, AGU, San Francisco, Calif., 13–17 Dec.
- Rahn, P. H. (1967), Sheetfloods, streamfloods, and the formation of pediments, *Ann. Assoc. Am. Geogr.*, 57(3), 593–604, doi:10.1111/j.1467-8306.1967.tb00624.x.
- Rajchenbach, J. (1990), Flow in powders: From discrete avalanches to continuous regime, *Phys. Rev. Lett.*, 65, 2221–2224, doi:10.1103/PhysRevLett.65.2221.
- Reddy, D. V., D. Kumar, D. Saha, and M. K. Mandal (2008), The 18 August 2008 Kosi river breach: An evaluation, *Curr. Sci.*, 95, 1668–1669.

- Reitz, M. D., D. J. Jerolmack, and J. B. Swenson (2010), Flooding and flow path selection on alluvial fans and deltas, *Geophys. Res. Lett.*, **37**, L06401, doi:10.1029/2009GL041985.
- Rosendahl, J., M. Vekic-slash, and J. Kelley (1993), Persistent self-organization of sandpiles, *Phys. Rev. E*, **47**(2), 1401–1404, doi:10.1103/PhysRevE.47.1401.
- Sambrook Smith, G., and R. Ferguson (1995), The gravel-sand transition along river channels, *J. Sediment. Res.*, **65**(2), 423–430.
- Savenije, H. (2003), The width of a bankful channel; Lacey's formula explained, *J. Hydrol.*, **276**, 176–183, doi:10.1016/S0022-1694(03)00069-6.
- Schumm, S., M. P. Mosley, and W. E. Weaver (1987), *Experimental Fluvial Geomorphology*, John Wiley, New York.
- Sheets, B., T. Hickson, and C. Paola (2002), Assembling the stratigraphic record: Depositional patterns and time-scales in an experimental alluvial basin, *Basin Res.*, **14**, 287–301, doi:10.1046/j.1365-2117.2002.00185.x.
- Slingerland, R., and N. Smith (2004), River avulsions and their deposits, *Annu. Rev. Earth Planet. Sci.*, **32**, 257–285, doi:10.1146/annurev.earth.32.101802.120201.
- Smith, N. D., T. A. Cross, J. P. Dufficy, and S. R. Clough (1989), Anatomy of an avulsion, *Sedimentology*, **36**, 1–23, doi:10.1111/j.1365-3091.1989.tb00817.x.
- Stock, J. D., K. M. Schmidt, and D. M. Miller (2008), Controls on alluvial fan long-profiles, *Geol. Soc. Am. Bull.*, **120**, 619–640, doi:10.1130/B26208.1.
- Stouthamer, E., and H. Berendsen (2001), Avulsion frequency, avulsion duration, and interavulsion period of Holocene channel belts in the Rhine-Meuse Delta, the Netherlands, *J. Sediment. Res.*, **71**, 589–598, doi:10.1306/112100710589.
- Straub, K. M., C. Paola, D. Mohrig, M. A. Wolinsky, and T. George (2009), Compensational stacking of channelized sedimentary deposits, *J. Sediment. Res.*, **79**, 673–688, doi:10.2110/jsr.2009.070.
- Swenson, J., V. Voller, C. Paola, G. Parker, and J. Marr (2000), Fluvio-deltaic sedimentation: A generalized Stefan problem, *Eur. J. Appl. Math.*, **11**, 433–452, doi:10.1017/S0956792500004198.
- Syvitski, J. P., and Y. Saito (2007), Morphodynamics of deltas under the influence of humans, *Global Planet. Change*, **57**, 261–282, doi:10.1016/j.gloplacha.2006.12.001.
- Syvitski, J., A. Kettner, A. Correggiari, and B. Nelson (2005), Distributary channels and their impact on sediment dispersal, *Mar. Geol.*, **222**, 75–94, doi:10.1016/j.margeo.2005.06.030.
- Syvitski, J., et al. (2009), Sinking deltas due to human activities, *Nat. Geosci.*, **2**, 681–686, doi:10.1038/ngeo629.
- Tang, C., and P. Bak (1988), Critical exponents and scaling relations for self-organized critical phenomena, *Phys. Rev. Lett.*, **60**, 2347–2350, doi:10.1103/PhysRevLett.60.2347.
- Törnqvist, T. E. (1994), Middle and late Holocene avulsion history of the River Rhine (Rhine-Meuse Delta, Netherlands), *Geology*, **22**, 711–714, doi:10.1130/0091-7613(1994)022<0711:MALHAH>2.3.CO;2.
- Wells, N., and J. Dorr (1987), Shifting of the Kosi River, Northern India, *Geology*, **15**, 204–207, doi:10.1130/0091-7613(1987)15<204:SOTKRN>2.0.CO;2.
- Whipple, K. X., G. Parker, C. Paola, and D. Mohrig (1998), Channel dynamics, sediment transport, and the slope of alluvial fans: Experimental study, *J. Geol.*, **106**, 677–694, doi:10.1086/516053.
- Wolinsky, M., D. Edmonds, J. Martin, and C. Paola (2010), Delta allometry: Growth laws for river deltas, *Geophys. Res. Lett.*, **37**, L21403, doi:10.1029/2010GL044592.
- Yalin, M. S., and E. Karahan (1979), Inception of sediment transport, *J. Hydraul. Div. Am. Soc. Civ. Eng.*, **105**, 1433–1443.